

---

# A Wearable Device Dataset for Mental Health Assessment Using Laser Doppler Flowmetry and Fluorescence Spectroscopy Sensors

---

Minh Ngoc Nguyen<sup>\*1,8</sup>, Khai Le-Duc<sup>\*2,3</sup>, Tan-Hanh Pham<sup>\*4</sup>,  
Trang Nguyen<sup>5</sup>, Quang Minh Luu<sup>6</sup>, Ba Kien Tran<sup>7</sup>, Truong-Son Hy<sup>9</sup>,  
Viktor Dremine<sup>1</sup>, Sergei Sokolovsky<sup>1</sup>, Edik Rafailov<sup>1</sup>

<sup>1</sup>Aston University, UK <sup>2</sup>University of Toronto, Canada <sup>3</sup>University Health Network, Canada

<sup>4</sup>Florida Institute of Technology, USA <sup>5</sup>Stanford University, USA

<sup>6</sup>108 Military Central Hospital, Vietnam <sup>7</sup>Hai Duong Central College of Pharmacy, Vietnam

<sup>8</sup>Industrial University of Ho Chi Minh City, Vietnam <sup>9</sup>University of Alabama at Birmingham, USA

Email: m.nguyen8@aston.ac.uk, duckkhai.le@mail.utoronto.ca

GitHub: [https://github.com/leduckkhai/Wearable\\_LDF-FS](https://github.com/leduckkhai/Wearable_LDF-FS)

## Abstract

In this study, we introduce a novel method to predict mental health by building machine learning models for a non-invasive wearable device equipped with Laser Doppler Flowmetry (LDF) and Fluorescence Spectroscopy (FS) sensors. Besides, we present the corresponding dataset to predict mental health, e.g. depression, anxiety, and stress levels via the DAS-21 questionnaire. To our best knowledge, this is the world's largest and the most generalized dataset ever collected for both LDF and FS studies. The device captures cutaneous blood microcirculation parameters, and wavelet analysis of the LDF signal extracts key rhythmic oscillations. The dataset, collected from 132 volunteers aged 18-94 from 19 countries, explores relationships between physiological features, demographics, lifestyle habits, and health conditions. We employed a variety of machine learning methods to classify stress detection, in which LightGBM is identified as the most effective model for stress detection, achieving a ROC AUC of 0.7168 and a PR AUC of 0.8852. In addition, we also incorporated Explainable Artificial Intelligence (XAI) techniques into our analysis to investigate deeper insights into the model's predictions. Our results suggest that females, younger individuals and those with a higher Body Mass Index (BMI) or heart rate have a greater likelihood of experiencing mental health conditions like stress and anxiety. All related code and data are published online: [https://github.com/leduckkhai/Wearable\\_LDF-FS](https://github.com/leduckkhai/Wearable_LDF-FS).

## 1 Introduction

### 1.1 Motivation

Over the past two decades, global incidences of Common Mental Disorders (CMDs), particularly anxiety and depression, have fluctuated significantly and increased substantially due to improved awareness and diagnosis in healthcare settings [1]. However, the increase in CMDs is not uniform across age groups, with higher rates among younger individuals due to changing social pressures and lifestyle factors[2]. Economic conditions and public health crises also influence mental health trends, highlighting the need for adaptable and accessible mental health services in the healthcare system.

---

\*Equal contribution

[3]. Mental health has gained significant attention, particularly after the COVID-19 pandemic, which exacerbated mental health issues [4, 5].

In the United Kingdom, over 25% of individuals experience a mental health disorder annually, with 1 in 6 adults facing anxiety or depression weekly<sup>1</sup>; stress leading to overeating (46%), increased alcohol consumption (29%), and elevated smoking rates (16%)<sup>2</sup>. CMDs harm various body systems, including raising blood pressure and heart risks in the cardiovascular system, impairing learning and mood in the nervous system, causing tension and fatigue in muscles, resulting in shallow breathing, and leading to weight changes and diabetes risk in metabolism. Ultimately, stress extensively affects both mental and physical well-being [6].

Stress can have a detrimental impact on various body systems [7]. Prolonged stress can elevate blood pressure and heart rate, increasing the risk of cardiovascular diseases [8]. It also affects the nervous system, leading to cognitive decline, mood disorders, and an increased risk of mental disorders [9]. Muscular tension, soreness, and fatigue can result from stress, impairing daily activities [10]. Changes in breathing patterns due to stress can lead to respiratory issues [11]. Additionally, stress disrupts metabolism, potentially causing weight changes and increasing the risk of diabetes [12]. In conclusion, stress negatively affects both mental and physical health, impacting systems such as cardiovascular, nervous, muscular, respiratory, and metabolic.

Mental health assessment encompasses various methods to ensure a comprehensive and accurate understanding. Standardized tests like DAS (Depression Anxiety Stress Scales) [13], the Beck Depression Inventory (BDI) [14], and the Beck Anxiety Inventory (BAI) [15] Clinical interviews, in structured, semi-structured, or unstructured formats, measure levels of depression, anxiety, and stress, helping psychologists gather detailed information through specific questions and conversations. Biological assessments, including tests for neurotransmitter levels like serotonin and dopamine, and electroencephalograms (EEGs) to monitor brain activity, also play a crucial role [16], and functional magnetic resonance imaging (fMRI) to observe brain activity during psychological tasks [17]. Biosensors for psychiatric biomarkers (e.g., cortisol, dopamine, serotonin) can diagnose and manage disorders via samples from blood, saliva, urine, and sweat. They offer high sensitivity, selectivity, and real-time monitoring, but face challenges like environmental accuracy, high costs, and data integration. Therefore, further development is needed for better effectiveness [18].

The DAS-21 questionnaire, a short version of the 42-item DAS, includes 21 items divided into three subscales: Depression, Anxiety, and Stress. It assesses motivation loss, anxiety symptoms, and irritability, respectively. Validated in clinical and community settings, the DAS-21 shows excellent internal consistency with Cronbach's alpha values of 0.94 for depression, 0.87 for anxiety, and 0.91 for stress. The DAS-21 severity levels and cutoff points classify and promptly support patients [19]. Intense emotions like anxiety or anger can affect the hands by altering blood flow and muscular electrical activity, causing muscle tension or relaxation [20]. Despite many articles on blood circulation in such individuals, none compare blood circulation variability in stressed vs. non-stressed people. This study demonstrated the wearable device's ability to differentiate cardiovascular parameters between stress and non-stress groups on both middle fingers.

Wearable devices with Laser Doppler Flowmetry (LDF) and Fluorescence Spectroscopy (FS) channels offer a promising approach for assessing microcirculation and obtaining comprehensive physiological and metabolic information. While these studies demonstrate their potential under normal and pathological conditions, further research with larger cohorts is essential for clinical implementation. One of the crucial tasks is to investigate the effects of various treatment protocols and lifestyle changes on microcirculatory and metabolic parameters using these wearable devices. Another important direction is to develop machine learning algorithms for automated data analysis and interpretation, which can significantly enhance the diagnostic capabilities of wearable devices. Our research focuses on building a diverse dataset for mental health detection using a non-invasive wearable device equipped with LDF and FS channels. By exploring subcutaneous blood microcirculation across demographics, we aim to provide valuable insights and pioneer the development of a large dataset for mental health assessment.

---

<sup>1</sup><https://www.mind.org.uk/news-campaigns/news/mind-urges-the-nation-speak-to-us-during-mental-health-awareness-week/>

<sup>2</sup><https://www.myndup.com/blog/mental-health-statistics-2023>

## 1.2 Literature Review

Professor E. Rafailov’s research group at Aston University has developed LDF/FS wearable devices using VCSEs, showing comparable signal responses to conventional monitors in volunteer assessments [21]. These devices employ LDF and FS for non-invasive early detection of vascular complications in diabetes and other conditions. LDF assesses tissue perfusion, oxygen saturation, and blood volume, while FS detects metabolic activity changes and AGEs accumulation, contributing to microvascular damage and inflammation in diabetes.

LDF is a non-invasive method for estimating perfusion in the microcirculation [22]. Introduced over 30 years ago, the technique uses laser radiation to probe tissue and analyze backscatter from moving red blood cells, primarily Hemoglobin (Hb). The main parameter recorded is the microcirculation or perfusion index, essential for organ nutrition, adaptation, and regulation. The method uses wavelet transformation, specifically adaptive wavelet analysis with complex-valued Morlet wavelets, to assess microvessel oscillatory processes over a wide frequency range. This has been the standard for over 15 years, replacing Fast Fourier Transform (FFT) and Butterworth filters [23]. Continuous wavelet transformation is preferred for non-stationary LDF-gram (perfusion) due to its optimal “time-frequency” resolution, effectively tracking frequency and amplitude fluctuations in blood flow signals [24]. The FS method uses laser probing to record fluorescence spectra of metabolic coenzymes, measuring NADH and FAD fluorescence intensity. This detects changes in metabolic activity in endothelial cells, indicating various physiological and pathological processes, and identifying cellular metabolic disorders related to diseases [25].

Several studies have utilized wearable devices to assess blood microcirculation across diverse patient groups. Older adults typically exhibit higher perfusion levels in areas like the middle palm and dorsal forearm due to thinner skin, aiding in diagnostic precision [24]. Conversely, younger individuals often show elevated wavelet parameters in blood perfusion oscillations, suggesting broad applicability in various pathologies. In endocrinology, wireless LDF devices have been used to evaluate microcirculatory function in type 2 diabetes patients and healthy individuals across different age brackets, revealing significant variations in perfusion levels [26]. Notably, studies monitoring diabetes patients receiving intravenous alpha-lipoic acid therapy have shown improvements in microcirculatory and nutritional blood flow, particularly in limbs affected by diabetic complications [27]. Additionally, wearable LDF devices have been instrumental in diagnosing vascular disorders during COVID-19 recovery, highlighting disruptions in microcirculatory function [28].

Further related works are described in Appendix Section A.

## 1.3 Contribution

In this study, we make three key contributions to the field of mental health assessment, placing particular emphasis on our data collection methods and the application of Explainable AI (XAI):

- **We present a novel approach for mental health assessment by establishing the largest and the most generalized dataset ever collected for both LDF and FS studies:** We address the need for robust datasets in the field by creating a novel data repository comprised of physiological signals captured using wearable devices. The dataset contains 132 patients, which is specifically chosen for its relevance to mental health and is further enriched by integrating self-reported DAS scores obtained through the validated depression, anxiety, and stress scale-21 (DAS-21) questionnaire.
- **Exploring numerous machine-learning algorithms for DAS prediction:** We move beyond traditional approaches that solely focus on achieving high prediction accuracy. We delve into the feasibility of utilizing various machine learning algorithms for predicting DAS levels.
- **Unveiling the “AI black box” by using XAI:** Recognizing the critical role of interpretability in mental health applications, we employ XAI techniques to investigate the decision-making behind a machine learning model. By employing XAI, we aim to illuminate the specific features within the wearable device data that exert the strongest influence on the health issues prediction of a person.

All related code and data are published online.

## 2 Study Design and Dataset Description

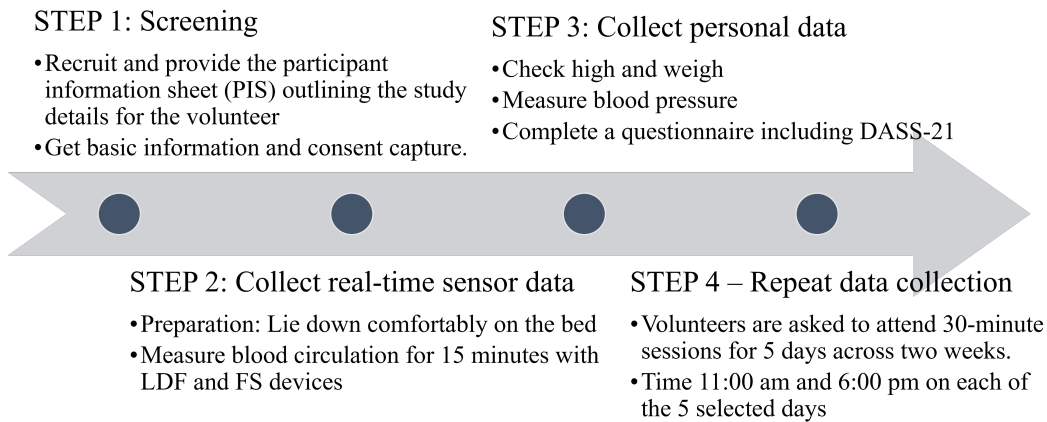


Figure 1: Data collection workflow.

There are four steps in data collection as shown in Fig. 1. Firstly, participants were recruited from the general population and included volunteers aged 18 and above. To ensure accurate blood perfusion measurements, individuals with any dermatological conditions on both hands and middle fingers were excluded from the study. Before commencing the study, all participants were provided with a detailed explanation of the study design and its objectives. After giving informed consent, participants completed a questionnaire detailing their current health status, including medication history, alcohol consumption within the past 24 hours, and exercise habits such as cycling, treadmill, or jogging.

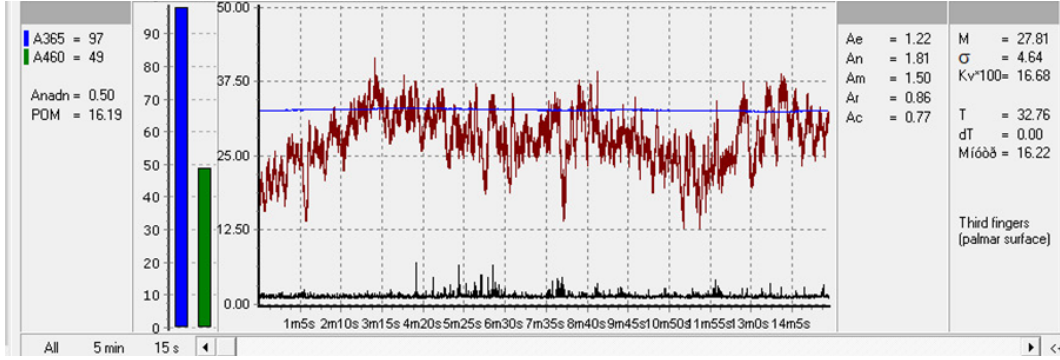
Sequentially, blood perfusion parameters were measured non-invasively with participants in a supine position to ensure physical and mental rest. To minimize external stimuli, participants were instructed to abstain from reading, writing, or talking during the test. Blood perfusion data were collected from sensors placed on the middle fingertips of both left and right hands for a duration of eight minutes. To control potential confounding factors, participants were asked to refrain from consuming caffeine and alcohol-containing drinks at least twelve hours before the designated measurement time.

Figure 2a shows the data measured from a stressed individual, with data from the left hand illustrated on the top and data from the right hand on the bottom. Similarly, Figure 2b presents an instance of well-being data collected using wearable devices. As observed, the data from the stressed individual exhibits significant fluctuations, while the data from the well-being individual is more stable. In addition, the definitions of the measurement device parameters are described following Table 1.

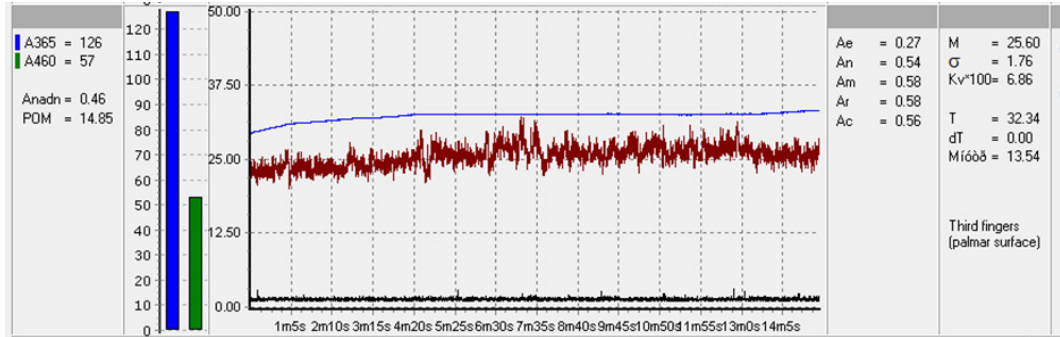
Following the 15-minute blood circulation measurement, we measured height and weight. Next, the participants completed the DAS-21 questionnaire, which assesses how much each statement applied to them over the past week. After completing the questionnaire, their blood pressure was measured. The measurements were taken twice a day: in the morning (around 11.00, before lunch) and in the afternoon (around 15.00, after lunch) for any five days over two consecutive weeks.

The DAS-21 is used to assess key symptoms of depression, anxiety, and stress, as well as patient reactions to treatment. It has been proven to have adequate psychometric properties and is equivalent to other accurate scales. The 21 items comprise three self-reported scales, each with seven elements graded on a Likert scale from 0 to 3. Depression, anxiety, and stress scores are measured by summing the scores of the related items. Since the DAS-21 is a shorter version of the original 42-item DAS, the score for each subscale must be multiplied by 2 to calculate the final score. Recommended cut-off scores for conventional severity labels (normal, moderate, severe) are calculated following Table 2. Scores on the DAS-21 will need to be multiplied by 2 to calculate the final score.

According to the manual, the ratings are classified as: “normal, mild, moderate, severe, or extremely severe”; all those who exhibit any signs of stress, anxiety, or depression, we referred to as the well-being group, and the remaining individuals will be classified as the wellbeing group. This allowed for real-time control of the course of the experiment and analysis of the recorded parameters.



(a) A stress instance of data collected using the wearable devices. The subject is a 36-year-old female with moderate stress, anxiety, and depression (right hand).



(b) An instance of well-being data collected using the wearable devices. The subject is a 27-year-old female (right hand).

Figure 2: Data instances collected using the wearable devices: (a) stress instance, (b) well-being instance.

The displayed parameters show the raw data of blood perfusion, temperature, and the movement of the fingertip and wrist. After acquiring the data, the oscillation rhythms of each measurement were analyzed using the built-in module “wavelet analysis”. This wavelet analysis determines the maximum amplitude of blood perfusion and corresponding data for each of the five oscillations: Five rhythmic oscillations are isolated from LDF recordings with the help of wavelet analysis; endothelial (frequency interval 0.0095–0.02 Hz), neurogenic (0.02–0.06 Hz), myogenic (0.06–0.16 Hz), respiratory (0.16–0.4 Hz), and cardiac or pulse rhythm (0.4–1.6 Hz).

As illustrated in Fig. 3, the total number of people with mental health issues reaches 27.3% of the population, with over 50% of them experiencing combined stress, anxiety, and depression. The incidence rates of stress, anxiety, and depression are 24.5%, 22%, and 18.2% respectively, mostly at mild levels, accounting for 17.2%, 13.6%, and 12.8% in these groups. The extremely severe level is highest in the anxiety group at 3.0%, while in the other two groups, it is below 1%.

Further details of data collection and data analysis are described in Appendix Section B.

### 3 Machine Learning and Explainable Artificial Intelligence

Further details of experimental setup are described in Appendix Section C.

#### 3.1 Machine Learning Models for DAS Prediction

To identify the most effective approach for predicting depression, anxiety, and stress levels, we explored various machine learning algorithms including Support Vector Machine (SVM), Random Forest Classification, Gradient Boosting Classifier, CatBoost, LightGBM, as well as Multi-layer Perceptron (MLP) [29]. In addition, we employ two primary approaches to train machine learning

Table 1: Definitions of the measurement device parameters.

| Parameters | Definition   |
|------------|--|
| M          | Microcirculation index, indicating the average perfusion of microvessels (in PU).  |
| $\sigma$   | Mean square deviation of blood flow oscillation amplitude (in PU).   |
| Kv         | Coefficient of blood flow variability.   |
| A365       | Backscatter amplitude at the laser source wavelength for NADH excitation.  |
| A460       | NADH fluorescence amplitude at 460 nm.   |
| NADH       | Relative amplitude of NADH fluorescence, considering the optical characteristics of the study tissue region.                   |
| POM        | Index of oxidative metabolism linked to the nutritional component of blood perfusion and NADH coenzyme fluorescence amplitude. |
| Ae         | Average maximum amplitude of blood flow within the endothelial oscillation range.  |
| An         | Average maximum amplitude of blood flow within the neurogenic oscillation range.   |
| Am         | Average maximum amplitude of blood flow within the myogenic oscillation range.   |
| Ar         | Average maximum amplitude of blood flow within the respiratory oscillation range.  |
| Ac         | Average maximum amplitude of blood flow within the cardiac oscillation range.  |
| Fe         | Endothelial oscillation frequency (0.0095 - 0.02 Hz).  |
| Fn         | Neurogenic oscillation frequency (0.02 - 0.06 Hz).   |
| Fm         | Myogenic oscillation frequency (0.06 - 0.16 Hz).   |
| Fr         | Respiratory oscillation frequency (0.16 - 0.4 Hz).   |
| Fc         | Cardiac oscillation frequency (0.4 - 1.6 Hz).  |
| T          | Temperature at the measurement site.   |

models for predicting DAS levels: binary classification and multi-class classification. Both approaches leverage data from the DAS-21 questionnaire alongside potentially other features from the collected dataset. In addition, we consider three cases to investigate the models' performances: Using all collected features, using only features extracted from wearable devices, and using top-10 important features.

For binary classification, this approach simplifies the prediction task by transforming the DAS levels into a binary classification problem. We categorize participants into two classes based on their DAS-21 scores:

- Normal: This class comprises participants who score within the normal range for depression, anxiety, and stress according to established DAS-21 scoring guidelines.
- Abnormal: This class encompasses participants whose DAS-21 scores indicate potential symptoms of depression, anxiety, or stress.

For multi-class classification, this approach aims for a more granular prediction by treating DAS levels as a multi-class classification problem. Instead of collapsing mental health states into two

Table 2: Scores on the DAS-21 will need to be multiplied by two to calculate the final score.

| Level            | Depression | Anxiety | stress |
|------------------|------------|---------|--------|
| Normal           | 0-9        | 0-7     | 0-14   |
| Mild             | 10-13      | 8-9     | 15-18  |
| Moderate         | 14-20      | 10-14   | 19-25  |
| Severe           | 21-27      | 15-19   | 26-33  |
| Extremely Severe | 28+        | 20+     | 34+    |

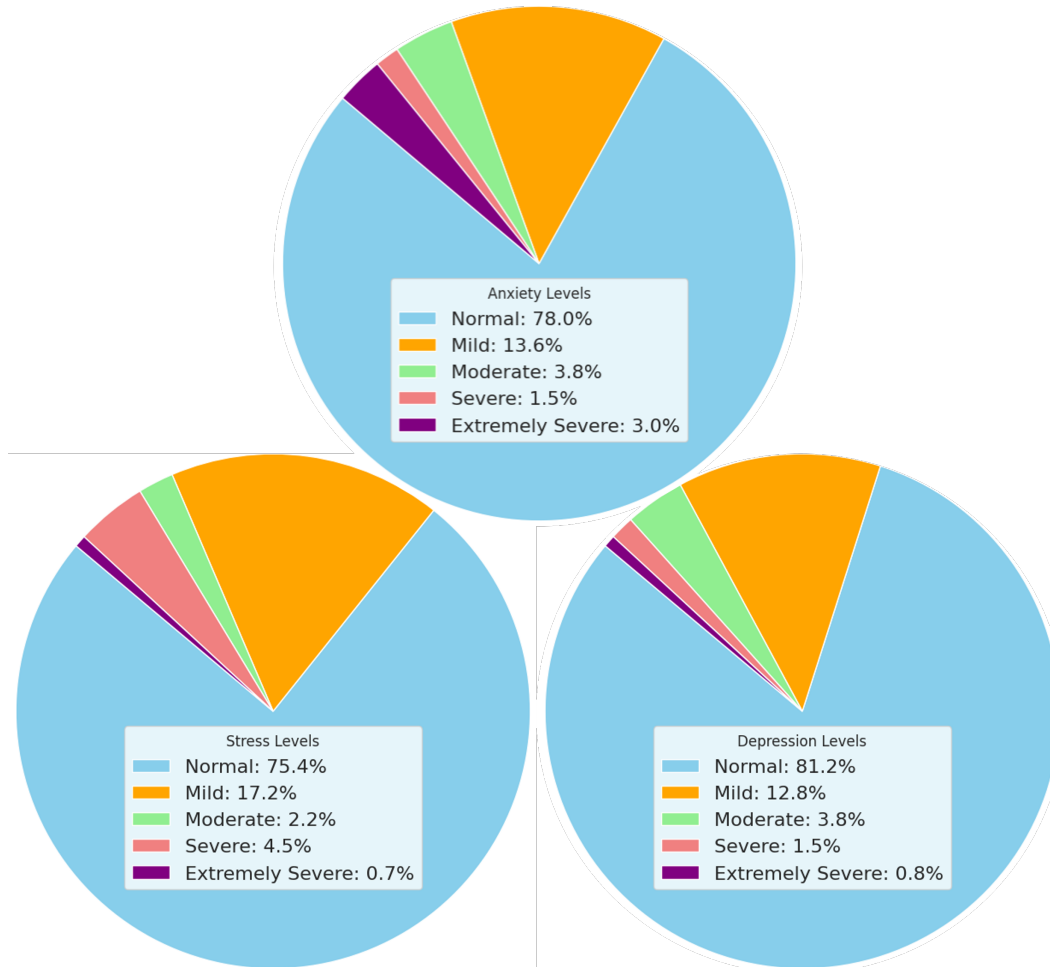


Figure 3: Distribution of stress levels, anxiety level, and depression level.

categories, we define multiple classes based on the established DAS-21 scoring ranges: Normal, stress, stress anxiety, and stress anxiety depression.

In machine learning, dividing the dataset into training and testing subsets is crucial for evaluating model performance. In our ablation study, we use three train-evaluate techniques: Split 80:20, patient-wise 5-folds (not sample-wise), and Leave-one-patient-out (LOPO) [30]. By doing this, we ensure that the model is evaluated on its ability to perform on new patients not seen during training.

To assess the performance of the machine learning models for predicting Depression, Anxiety, and stress (DAS) levels, we employ two key evaluation metrics: Receiver Operating Characteristic (ROC) AUC (Area Under the Curve) and Precision-Recall (PR) AUC. These metrics provide a comprehensive assessment of the model's discriminative ability and its performance in handling class imbalances.

### 3.2 Explainable AI

In healthcare applications, understanding the reasoning behind a model’s predictions for DAS levels is crucial for building trust and confidence in its outputs. This empowers healthcare professionals and researchers to make informed decisions based on the predicted DAS levels and the underlying factors influencing those predictions. In this study, we leverage SHAP (Shapley Additive Explanations) to achieve interpretability and gain insights into the model’s decision-making process for DAS prediction [31]. SHAP assigns an attribution value (SHAP value) to each feature for a given DAS prediction. High positive SHAP values indicate that the feature has a strong positive influence on the predicted DAS level (potentially indicating a higher likelihood of depression, anxiety, or stress). Conversely, low negative SHAP values signify a negative influence (indicating a lower likelihood). This interpretability allows us to answer several key questions:

- Identification of the key physiological and psychological indicators: What are the features from wearable sensor data and questionnaire scores of a patient that have the most significant influence on the model’s predictions?
- Validation of model fairness and mitigation of bias: Are the model’s predictions fair across different demographics (age, gender, etc.)? Examining SHAP values across these groups helps ensure that the model is not unfairly biased toward certain populations.
- Enhanced model transparency: How does the model arrive at its predictions? By explaining the rationale behind the model’s predictions through SHAP values, we can foster trust and confidence in its use among healthcare professionals and researchers.

## 4 Experimental Results

### 4.1 All Features with 80:20 Split

In this section, we present the results of our investigation into using machine learning models to predict stress levels based on data from the DAS-21 questionnaire and potentially other features within our dataset. We employed both binary and multi-class classification approaches, evaluating the models on a random 80/20 train-test split to ensure generalizability.

#### 4.1.1 Binary Classification

Our initial focus was on a binary classification task, aiming to identify individuals with potential mental health concerns based on their DAS-21 scores. For binary classification, the performance of the models on binary classification tasks is summarized in Table 3.

From the table, LightGBM emerged as the best-performing model, achieving the highest ROC AUC of 0.9941 and PR AUC of 0.9982. Gradient Boosting and MLP also demonstrated strong performance, with ROC AUC values of 0.9751 and 0.9322, respectively. In contrast, Catboost and Random Forest showed relatively lower performance, indicating that they might not be as effective for this particular binary classification task.

Table 3: Performance for different models: All features with 80:20 split, binary classification

| Model          | Gradient Boosting | Catboost | LightGBM | SVM    | Random Forest | MLP    |
|----------------|-------------------|----------|----------|--------|---------------|--------|
| <b>ROC AUC</b> | 0.9751            | 0.7320   | 0.9941   | 0.9199 | 0.8145        | 0.9322 |
| <b>PR AUC</b>  | 0.9911            | 0.9104   | 0.9982   | 0.9720 | 0.9330        | 0.9767 |

#### 4.1.2 Multi-class Classification

In addition to predicting whether a person has a mental issue or not, we also explored a multi-class classification task, aiming to predict not only the presence of stress but also its severity level. In particular, Table 4 details the performance metrics of the models on multi-class classification tasks, with the notable absence of MLP results.



Table 4: Performance for different models: All features with 80:20 split, multi-class classification

| Model                            | Gradient Boosting | Catboost | LightGBM | SVM    | Random Forest |
|----------------------------------|-------------------|----------|----------|--------|---------------|
| <b>Macro ROC AUC One-vs-Rest</b> | 0.8043            | 0.6932   | 0.9962   | 0.973  | 0.8695        |
| <b>Macro ROC AUC One-vs-One</b>  | 0.8302            | 0.6875   | 0.993    | 0.9574 | 0.7952        |
| <b>Macro Precision</b>           | 0.6238            | 0.1723   | 0.9875   | 0.4417 | 0.2966        |
| <b>Recall</b>                    | 0.5319            | 0.2108   | 0.9085   | 0.3799 | 0.1845        |
| <b>F1-score</b>                  | 0.5152            | 0.1808   | 0.9391   | 0.375  | 0.1783        |

LightGBM again stands out, achieving near-perfect Macro ROC AUC scores and high precision, recall, and F1 scores. Gradient Boosting and SVM also performed well, with Gradient Boosting showing a balanced performance across all metrics. Catboost and Random Forest had lower scores, suggesting limitations in handling the complexities of multi-class classification in this context.

Table 5: Top 10 important features using Gradient Boosting, Catboost, and LightGBM when conducting binary prediction with an 80:20 split. The meaning of each feature is explained in Table 1.

| Order | Gradient Boosting |            | Catboost        |            | LightGBM      |            |
|-------|-------------------|------------|-----------------|------------|---------------|------------|
|       | Feature           | Importance | Feature         | Importance | Feature       | Importance |
| 1     | BMI_index         | 0.279819   | Age             | 55.244066  | BMI_index     | 22         |
| 2     | Heart Rate        | 0.163589   | Type of skins   | 29.933423  | Heart Rate    | 13         |
| 3     | Age               | 0.160837   | Weight          | 11.040225  | Age           | 13         |
| 4     | Type of skins     | 0.156214   | $\delta$        | 3.782286   | Weight        | 9          |
| 5     | Weight            | 0.097077   | Type of data    | 0.000000   | Height        | 8          |
| 6     | T                 | 0.050864   | F_Ae            | 0.000000   | M             | 6          |
| 7     | Height            | 0.044463   | Level of BP     | 0.000000   | T             | 6          |
| 8     | A460              | 0.011797   | Smoking routine | 0.000000   | A460          | 5          |
| 9     | Anadn             | 0.009720   | BMI_index       | 0.000000   | Kv100         | 2          |
| 10    | M                 | 0.009113   | Height          | 0.000000   | Type of skins | 2          |

### 4.1.3 Feature Importance

To understand the factors influencing the models' predictions, we analyzed the importance of various features. Feature importance was assessed using Gradient Boosting, Catboost, and LightGBM models, as summarized in Table 5 and 6. The tables highlight the top 10 important features identified by each model. In both tables, features such as heart rate, BMI, weight, T (temperature), and type of skin consistently rank high in the top ten importance for most models. This suggests that physiological factors significantly influence the models' stress predictions. Other features including age, POM, A365, and Anadn also appear to be relevant to some degree, depending on the model.

## 4.2 All Features with Cross-Validation

In the field of health issue analysis, ensuring the robustness and reliability of predictive models is paramount. To achieve this, we employ cross-validation techniques such as k-fold cross-validation and LOPO cross-validation.

Table 6: Top 10 important features using Gradient Boosting, Catboost, and LightGBM for multi-class classification with an 80:20 split. The meaning of each feature is explained in Table 1.

| Order | Gradient Boosting |            | Catboost        |            | LightGBM      |            |
|-------|-------------------|------------|-----------------|------------|---------------|------------|
|       | Feature           | Importance | Feature         | Importance | Feature       | Importance |
| 1     | Heart Rate        | 0.682942   | Heart Rate      | 87.150766  | Weight        | 18         |
| 2     | A365              | 0.179464   | Type of skins   | 8.122651   | Height        | 9          |
| 3     | BMI_index         | 0.089107   | Anadn           | 3.149739   | BMI_index     | 8          |
| 4     | Type of skins     | 0.043119   | $\delta$        | 1.576843   | Heart Rate    | 7          |
| 5     | Height            | 0.004020   | F_An            | 0.000000   | Type of skins | 7          |
| 6     | Age               | 0.001002   | Level of BP     | 0.000000   | A365          | 7          |
| 7     | POM               | 0.000173   | Smoking routine | 0.000000   | Age           | 5          |
| 8     | T                 | 0.000173   | BMI_index       | 0.000000   | POM           | 5          |
| 9     | F_An              | 0.000000   | Height          | 0.000000   | T             | 5          |
| 10    | Level of BP       | 0.000000   | Weight          | 0.000000   | F_Ar          | 2          |

#### 4.2.1 Binary Classification with LOPO

LOPO cross-validation is particularly relevant in medical studies, where patient-specific variations can significantly impact the model’s predictions. Table 7 presents the performance metrics for various machine learning models when evaluated using the LOPO cross-validation method for binary classification. LOPO is a stringent evaluation method where the model is trained on all patients except one, who is then used as the test set. This process is repeated for each patient, ensuring that the model’s performance is tested on unseen data in each iteration.

Table 7: Performance for different models: All features with LOPO, binary classification.

| Model          | Gradient Boosting | Catboost | LightGBM | SVM    | Random Forest | MLP    |
|----------------|-------------------|----------|----------|--------|---------------|--------|
| <b>ROC AUC</b> | 0.6556            | 0.6001   | 0.6773   | 0.5316 | 0.6209        | 0.5313 |
| <b>PR AUC</b>  | 0.8806            | 0.8287   | 0.8998   | 0.8214 | 0.8630        | 0.8425 |

From the results, LightGBM shows the highest ROC AUC (0.6773) and PR AUC (0.8998), indicating better performance in distinguishing between the two classes compared to other models. Gradient Boosting and Random Forest also perform reasonably well, with ROC AUC values of 0.6556 and 0.6209, respectively. SVM and MLP perform the worst in terms of ROC AUC, indicating they might struggle more with the variability in the patient data.

#### 4.2.2 Binary Classification with 5-folds

As mentioned above, we also use 5-fold cross-validation to investigate the performance of the models. In 5-fold cross-validation, the dataset is divided into 5 subsets, and the model is trained and tested k times, each time using a different subset as the validation set and the remaining subsets for training, providing a thorough assessment of the model’s performance. This method helps to mitigate overfitting and ensures that the model is not overly dependent on any particular subset of the data.

Table 8 provides the performance metrics for the same machine learning models but evaluated using 5-fold cross-validation. In this method, the dataset is split into five equal parts, and the model is trained on four parts and tested on the remaining one. This process is repeated five times, with each part used exactly once as the test set.

In this evaluation, LightGBM again outperforms other models with a ROC AUC of 0.6892 and a PR AUC of 0.8833. Gradient Boosting and Random Forest show comparable ROC AUC values of

Table 8: Performance for different models: All features with 5-fold, binary classification.

| Model          | Gradient Boosting | Catboost | LightGBM | SVM    | Random Forest | MLP    |
|----------------|-------------------|----------|----------|--------|---------------|--------|
| <b>ROC AUC</b> | 0.6292            | 0.5462   | 0.6892   | 0.5571 | 0.6257        | 0.5182 |
| <b>PR AUC</b>  | 0.8529            | 0.8255   | 0.8833   | 0.8184 | 0.8597        | 0.8318 |

0.6292 and 0.6257, respectively. Catboost and SVM exhibit lower performance, while MLP remains the lowest-performing model based on ROC AUC.

#### 4.2.3 Multi-class Classification with LOPO

In addition to the binary classification, we also investigate the performance of models' prediction using multi-level severity following DAS21. Table 9 details the performance of the models on multi-class classification tasks using the LOPO cross-validation. The approach is even more challenging in a multi-class setting as the model must correctly classify multiple classes for each patient left out during testing.

Table 9: Performance for different models: All features with LOPO, multi-class classification.

| Model                                      | Gradient Boosting | Catboost | LightGBM | SVM    | Random Forest |
|--|-------------------|----------|----------|--------|---------------|
| <b>Macro ROC AUC</b><br><b>One-vs-Rest</b> | 0.4466            | 0.3279   | 0.5678   | 0.4208 | 0.3092        |
| <b>Macro ROC AUC</b><br><b>One-vs-One</b>  | 0.4197            | 0.336    | 0.4781   | 0.4237 | 0.2767        |
| <b>Macro Precision</b>                     | 0.1719            | 0.1346   | 0.1336   | 0.1311 | 0.1317        |
| <b>Recall</b>                              | 0.1776            | 0.1384   | 0.1493   | 0.1631 | 0.1667        |
| <b>F1-score</b>                            | 0.1698            | 0.1307   | 0.1408   | 0.1454 | 0.1472        |

LightGBM exhibits the best performance for multi-class classification with LOPO, achieving a Macro ROC AUC of 0.5678 in the One-vs-Rest approach and 0.4781 in the One-vs-One approach. However, all models show relatively low performance across all metrics, reflecting the difficulty of the multi-class classification task under LOPO validation.

#### 4.2.4 Multi-class Classification with 5-folds

Similar to the LOPO for multi-class classification, we also employ 5-fold for health issue investigation. Table 10 shows the performance metrics for multi-class classification using 5-fold cross-validation. This method helps mitigate the variance seen in LOPO by averaging the performance over multiple splits.

Table 10: Performance for different models: All features with 5-fold, multi-class classification.

| Model                                      | Gradient Boosting | Catboost | LightGBM | SVM    | Random Forest |
|--|-------------------|----------|----------|--------|---------------|
| <b>Macro ROC AUC</b><br><b>One-vs-Rest</b> | 0.4804            | 0.4103   | 0.5812   | 0.4412 | 0.4663        |
| <b>Macro ROC AUC</b><br><b>One-vs-One</b>  | 0.4492            | 0.4132   | 0.5057   | 0.4539 | 0.4207        |
| <b>Macro Precision</b>                     | 0.1783            | 0.1434   | 0.1554   | 0.1357 | 0.1223        |
| <b>Recall</b>                              | 0.1746            | 0.1539   | 0.1652   | 0.1628 | 0.1667        |
| <b>F1-score</b>                            | 0.1736            | 0.1474   | 0.1578   | 0.1465 | 0.1411        |

Table 10 shows that LightGBM continues to show the highest performance with a Macro ROC AUC of 0.5812 (One-vs-Rest) and 0.5057 (One-vs-One). Gradient Boosting and SVM also perform relatively well, but all models have lower performance metrics compared to the binary classification tasks, illustrating the increased complexity of multi-class classification.

### 4.3 Multimodal Sensor Features

#### 4.3.1 Binary Classification with LOPO

The performance metrics for different machine learning models using the LOPO approach are summarized in Table 11. The LightGBM model achieved the highest ROC AUC score of 0.698, suggesting it performed relatively better compared to using all features as illustrated in Table 7. Gradient Boosting followed with an ROC AUC of 0.6265, indicating moderate discriminative ability. In terms of PR AUC, which measures the trade-off between precision and recall, LightGBM again stands out with a score of 0.9091, demonstrating its robustness in handling imbalanced classes. Other models including Catboost, SVM, and Random Forest showed lower ROC AUC and PR AUC scores.

Table 11: Performance for different models: Multimodal sensor features with LOPO, binary classification.

| Model          | Gradient Boosting | Catboost | LightGBM | SVM    | Random Forest | MLP    |
|----------------|-------------------|----------|----------|--------|---------------|--------|
| <b>ROC AUC</b> | 0.6265            | 0.4753   | 0.698    | 0.5124 | 0.556         | 0.5034 |
| <b>PR AUC</b>  | 0.8379            | 0.7556   | 0.9091   | 0.8113 | 0.8209        | 0.7855 |

#### 4.3.2 Binary Classification with 5-folds

The performance metrics for the 5-fold cross-validation approach are detailed in Table 12. Here, LightGBM also performed well, achieving an ROC AUC of 0.6601 and a PR AUC of 0.8839, highlighting its consistent performance across different validation techniques. Gradient Boosting followed with an ROC AUC of 0.6137 and a PR AUC of 0.8424, reinforcing its reliability as a robust model for this classification task. The Catboost model showed improved performance in the 5-fold scenario (ROC AUC of 0.5145) compared to LOPO, indicating that it might be better suited for general datasets rather than patient-specific variations. SVM and Random Forest had similar ROC AUC scores, around 0.5389 and 0.5607 respectively, but they showed adequate precision-recall trade-offs with PR AUC scores above 0.82.

Table 12: Performance for different models: Multimodal sensor features with 5-fold, binary classification.

| Model          | Gradient Boosting | Catboost | LightGBM | SVM    | Random Forest | MLP    |
|----------------|-------------------|----------|----------|--------|---------------|--------|
| <b>ROC AUC</b> | 0.6137            | 0.5145   | 0.6601   | 0.5389 | 0.5607        | 0.5216 |
| <b>PR AUC</b>  | 0.8424            | 0.7914   | 0.8839   | 0.8207 | 0.8261        | 0.7983 |

### 4.4 Top-10 Important Features

Although, we have features extracted from wearable devices and personal information, utilizing the top 10 important features for classification is a strategic approach aimed at enhancing model efficiency and interpretability. Utilizing the top 10 important features allows us to significantly reduce the time and energy required for data collection and processing, thereby saving valuable resources and expediting the overall analysis workflow.

#### 4.4.1 Binary Classification with LOPO

As shown in Table 13, the models assessed include Gradient Boosting, Catboost, LightGBM, SVM, Random Forest, and MLP. The results indicate that LightGBM achieved the highest ROC AUC score of 0.7041, followed by Gradient Boosting with a score of 0.6699. Catboost, SVM, Random Forest, and MLP showed moderate performance with ROC AUC scores of 0.5788, 0.578, 0.6232, and 0.5454, respectively. In addition, in terms of Precision-Recall AUC, LightGBM also led with a score of 0.9087, highlighting its superior ability to handle class imbalances and correctly identify positive instances in this binary classification task.

Table 13: Performance for different models: Top 10 features with LOPO, binary classification.

| Model          | Gradient Boosting | Catboost | LightGBM | SVM    | Random Forest | MLP    |
|----------------|-------------------|----------|----------|--------|---------------|--------|
| <b>ROC AUC</b> | 0.6699            | 0.5788   | 0.7041   | 0.578  | 0.6232        | 0.5454 |
| <b>PR AUC</b>  | 0.8689            | 0.8213   | 0.9087   | 0.8591 | 0.8714        | 0.8413 |

#### 4.4.2 Binary Classification with 5-folds

LightGBM consistently performed well, achieving an ROC AUC of 0.7168 and a PR AUC of 0.8852, underscoring its robustness and effectiveness across different cross-validation techniques. Gradient Boosting and Catboost also performed competitively with ROC AUC scores of 0.6594 and 0.6173, respectively, and PR AUC scores of 0.8723 and 0.8512.

Table 14: Performance for different models: Top 10 features with 5-fold, binary classification.

| Model          | Gradient Boosting | Catboost | LightGBM | SVM    | Random Forest |
|----------------|-------------------|----------|----------|--------|---------------|
| <b>ROC AUC</b> | 0.6594            | 0.6173   | 0.7168   | 0.5692 | 0.6402        |
| <b>PR AUC</b>  | 0.8723            | 0.8512   | 0.8852   | 0.841  | 0.8754        |

#### 4.4.3 Multi-class Classification with LOPO

We also conducted multi-class classification training using the LOPO method. As shown in Table 15, the performance metrics indicate a notable variation among the machine learning models. LightGBM emerged as the top performer with a Macro ROC AUC score of 0.633 (One-vs-Rest) and 0.5244 (One-vs-One), demonstrating its capability to handle multiple classes effectively. Gradient Boosting and Catboost showed moderate performance with Macro ROC AUC scores around 0.4946 and 0.4463, respectively. However, the overall macro precision, recall, and F1-score for all models were relatively low, highlighting the complexity and challenge of multi-class classification tasks using LOPO.

Table 15: Performance for different models: Top 10 features with LOPO, multi-class classification.

| Model                            | Gradient Boosting | Catboost | LightGBM | SVM    | Random Forest |
|----------------------------------|-------------------|----------|----------|--------|---------------|
| <b>Macro ROC AUC One-vs-Rest</b> | 0.4946            | 0.4463   | 0.633    | 0.4466 | 0.3352        |
| <b>Macro ROC AUC One-vs-One</b>  | 0.4933            | 0.4084   | 0.5244   | 0.4344 | 0.3007        |
| <b>Macro Precision</b>           | 0.1935            | 0.1558   | 0.1636   | 0.1335 | 0.1317        |
| <b>Recall</b>                    | 0.2182            | 0.1737   | 0.1742   | 0.1552 | 0.1667        |
| <b>F1-score</b>                  | 0.1947            | 0.159    | 0.1679   | 0.1429 | 0.1472        |

#### 4.4.4 Multi-class Classification with 5-folds

Finally, we conducted multi-class classification using the same models with 5-fold cross-validation. Table 16 shows that LightGBM again led with a Macro ROC AUC score of 0.6412 (One-vs-Rest) and 0.5585 (One-vs-One), reinforcing its consistent performance across different evaluation methods. Gradient Boosting and Catboost also showed improved performance with Macro ROC AUC scores of 0.5418 and 0.5315, respectively.

When employing the top 10 features, the binary classification performance under the LOPO scheme shows a slightly better performance in ROC AUC and PR AUC metrics across most models compared to using all features. For example, Gradient Boosting’s ROC AUC increased from 0.6556 to 0.6699, while LightGBM’s PR AUC slightly increased from 0.8998 to 0.9087. Similarly, in multi-class classification, the LOPO results show that models trained with the top 10 features generally have higher Macro ROC AUC and precision scores compared to those trained with all features. By focusing on the top ten important features, we can not only enhance model performance but also significantly reduce the time and energy required for data collection and processing, making the analysis more efficient and cost-effective.

Table 16: Performance for different models: Top 10 features with 5-fold, multi-class classification.

| Model                  | Gradient Boosting | Catboost | LightGBM | SVM    | Random Forest |
|------------------------|-------------------|----------|----------|--------|---------------|
| <b>Macro ROC AUC</b>   |                   |          |          |        |               |
| <b>One-vs-Rest</b>     | 0.5418            | 0.5315   | 0.6412   | 0.5022 | 0.3857        |
| <b>Macro ROC AUC</b>   |                   |          |          |        |               |
| <b>One-vs-One</b>      | 0.5507            | 0.4474   | 0.5585   | 0.4755 | 0.3615        |
| <b>Macro Precision</b> | 0.2314            | 0.1401   | 0.1778   | 0.1525 | 0.2896        |
| <b>Recall</b>          | 0.2347            | 0.1476   | 0.2031   | 0.1705 | 0.1711        |
| <b>F1-score</b>        | 0.2224            | 0.1416   | 0.1885   | 0.1596 | 0.1502        |

### 4.5 Health Issue Explanation

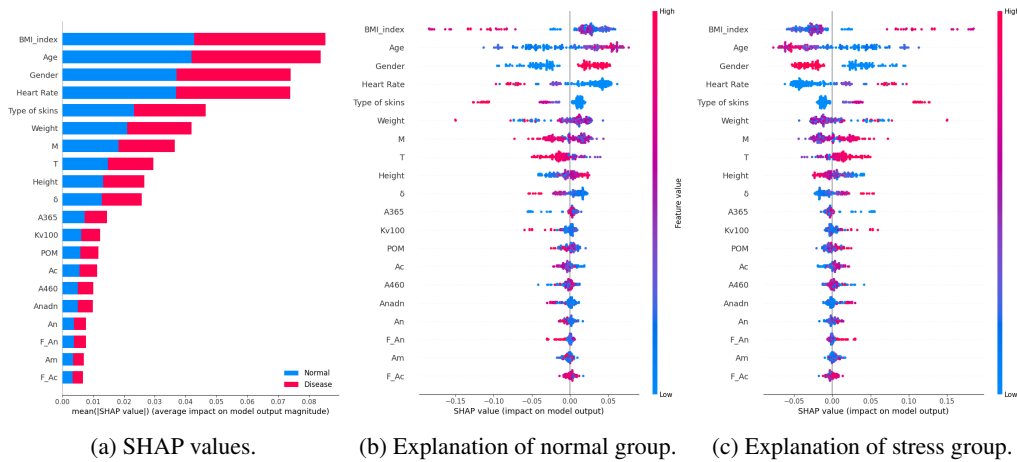


Figure 4: Explanation of the reasoning behind individual class predictions using SHAP values.

While in the previous sections, we focused on the performance of various machine learning models for health issue prediction, it’s crucial to understand the underlying factors influencing these predictions. This is where Explainable Artificial Intelligence (XAI) techniques come into play. XAI methods enable us to gain insights into the decision-making processes of machine learning models, offering valuable explanations for their predictions. As discussed in Section 4.1 to Section 4.4, LightGBM outperforms other machine learning models. Therefore, we employed XAI techniques to interpret the top-performing LightGBM model for stress detection.

A plot of the SHAP values is illustrated in Fig. 4a, in which the features are listed on the left-hand side of the plot, with the most important features at the top. Higher SHAP values indicate a greater impact on the model output. In addition, the blue color represents the normal class and the red color is the stress class. As we can see, BMI index is the most important feature, followed by age, gender, and heart rate. As we can see, the contribution of each feature in each class is mostly equal.

To understand the distribution of each feature in each class, we plot the SHAP values of each class in Fig. 4b and Fig. 4c. Similar to Fig. 4a, the images show scatter plots of the effects of factors on model output for each class. The x-axis represents the feature value, and the y-axis represents the SHAP value. As observed a low BMI index is associated with a lower likelihood of being classified as stressed by the model. Similar to the BMI index, Fig. 4c shows high age and low heart rate are indicative of a lower likelihood of being stressed according to the model. In addition, females seem to be more stressed than males.

## 5 Conclusion

In this study, we introduce a novel approach to predict mental health by training predictive machine learning models for a non-invasive wearable device equipped with LDF/FS sensors. Also, we establish

a large, novel wearable device dataset containing physiological signals and corresponding DAS-21 scores. To our best knowledge, this is the largest and the most generalized dataset ever collected for both LDF and FS studies. Additionally, we also evaluated various machine learning models for predicting DAS levels, prioritizing interpretable models to enhance understanding of the relationship between wearable data and mental health. Finally, we employed explainable AI techniques to ensure transparency by identifying features that most influence predictions, providing insights that can help clinicians tailor treatment plans and improve patient outcomes.

Our findings show that: (1) The LightGBM model consistently outperforms others in both binary and multi-class stress level predictions, balancing accuracy and interpretability, making it suitable for practical applications. Using the top 10 important features, LightGBM achieved an ROC AUC of 0.7168 and a PR AUC of 0.8852. (2) Key physiological features like heart rate, BMI, and weight significantly influence stress predictions. (3) Younger individuals and those with a higher BMI or heart rate have a higher chance of experiencing stress. (4) Females are more likely to be stressed than males.

## **6 Acknowledgement**

We would like to extend our sincere appreciation to the Human ethics committee at Aston University, Birmingham, UK and Hai Duong central college of pharmacy, Vietnam, for their support and cooperation, including the waiver of informed consent. Their dedication to ethical standards greatly contributed to the success of this study.

Authors also acknowledge support from the British Council Women in STEM Fellowships program (grants No. 2324).

## References

- [1] Yang Wu, Lu Wang, Mengjun Tao, Huiru Cao, Hui Yuan, Mingquan Ye, Xingui Chen, Kai Wang, and Chunyan Zhu. Changing trends in the global burden of mental disorders from 1990 to 2019 and predicted levels in 25 years. *Epidemiology and Psychiatric Sciences*, 32:e63, 2023.
- [2] Steinar Krokstad, Daniel Albert Weiss, Morten Austheim Krokstad, Vegar Rangel, Kirsti Kvaløy, Jo Magne Ingul, Ottar Bjerkeset, Jean Twenge, and Erik R Sund. Divergent decennial trends in mental health according to age reveal poorer mental health for young people: repeated cross-sectional population-based surveys from the hunt study, norway. *BMJ open*, 12(5): e057654, 2022.
- [3] J Dykxhoorn, D Osborn, K Walters, JB Kirkbride, S Gnani, and AI Lazzarino. Temporal patterns in the recorded annual incidence of common mental disorders over two decades in the united kingdom: A primary care cohort study. *Psychological Medicine*, 54(4):663–674, 2024.
- [4] Klaus W Lange. Coronavirus disease 2019 (covid-19) and global mental health. *Global health journal*, 5(1):31–36, 2021.
- [5] Lola Kola, Brandon A Kohrt, Charlotte Hanlon, John A Naslund, Siham Sikander, Madhumitha Balaji, Corina Benjet, Eliza Yee Lai Cheung, Julian Eaton, Pattie Gonsalves, et al. Covid-19 mental health impact and responses in low-income and middle-income countries: reimagining global mental health. *The Lancet Psychiatry*, 8(6):535–550, 2021.
- [6] Esme Kirk-Wade Carl Baker. Mental health statistics: prevalence, services and funding in england. *commonslibrary.parliament.uk*, Number CBP-06988:1–44, 2024.
- [7] George P Chrousos. Stress and disorders of the stress system. *Nature reviews endocrinology*, 5(7):374–381, 2009.
- [8] Andrew Steptoe and Mika Kivimäki. Stress and cardiovascular disease. *Nature Reviews Cardiology*, 9(6):360–370, 2012.
- [9] Francesca Calabrese, Raffaella Molteni, Giorgio Racagni, and Marco A Riva. Neuronal plasticity: a link between stress and mood disorders. *Psychoneuroendocrinology*, 34:S208–S216, 2009.
- [10] Waleed Umer, Yantao Yu, and Maxwell Fordjour Antwi Afari. Quantifying the effect of mental stress on physical stress for construction tasks. *Journal of Construction Engineering and Management*, 148(3):04021204, 2022.
- [11] Anette Pedersen, Robert Zachariae, and Dana H Bovbjerg. Influence of psychological stress on upper respiratory infection—a meta-analysis of prospective studies. *Psychosomatic medicine*, 72(8):823–832, 2010.
- [12] Melissa L Harris, Christopher Oldmeadow, Alexis Hure, Judy Luu, Deborah Loxton, and John Attia. Stress increases the risk of type 2 diabetes onset in women: A 12-year longitudinal study using causal modelling. *PloS one*, 12(2):e0172126, 2017.
- [13] Sydney H Lovibond and Peter F Lovibond. Depression anxiety stress scales. *Psychological Assessment*, 1995.
- [14] Aaron T Beck, Robert A Steer, and Gregory K Brown. Beck depression inventory. *San Antonio, TX*, 1987.
- [15] Aaron T Beck, Norman Epstein, Gary Brown, and Robert Steer. Beck anxiety inventory. *Journal of consulting and clinical psychology*, 1993.
- [16] Priya Miranda, Christopher D Cox, Michael Alexander, Slav Danev, and Jonathan RT Lakey. Overview of current diagnostic, prognostic, and therapeutic use of eeg and eeg-based markers of cognition, mental, and brain health. *Integrative Molecular Medicine*, 6:1–9, 2019.
- [17] Lori A Whitten. Functional magnetic resonance imaging (fmri): An invaluable tool in translational neuroscience. 2012.



- [18] Lin Wang, Yubing Hu, Nan Jiang, and Ali K Yetisen. Biosensors for psychiatric biomarkers in mental health monitoring. *Biosensors and Bioelectronics*, page 116242, 2024.
- [19] Renan P Monteiro, Gabriel Lins de Holanda Coelho, Paul HP Hanel, Valdiney V Gouveia, and Roosevelt Vilar. The 12-item mini-dass: A concise and efficient measure of depression, anxiety, and stress. *Applied Research in Quality of Life*, 18(6):2955–2979, 2023.
- [20] James L McGaugh. *Emotions and bodily responses: A psychophysiological approach*. Academic Press, 2013.
- [21] Evgeny A Zherebtsov, Elena V Zharkikh, Igor Kozlov, Angelina I Zherebtsova, Yulia I Loktionova, Nikolay B Chichkov, Ilya E Rafailov, Victor V Sidorov, Sergei G Sokolovski, Andrey V Dunaev, et al. Novel wearable vcsel-based sensors for multipoint measurements of blood perfusion. In *Dynamics and Fluctuations in Biomedical Photonics XVI*, volume 10877, pages 38–41. SPIE, 2019.
- [22] David A Low, Helen Jones, N Tim Cable, Lacy M Alexander, and W Larry Kenney. Historical reviews of the assessment of human cardiovascular function: interrogation and understanding of the control of skin blood flow. *European Journal of Applied Physiology*, 120:1–16, 2020.
- [23] Lana Kralj and Helena Lenasi. Wavelet analysis of laser doppler microcirculatory signals: Current applications and limitations. *Frontiers in Physiology*, 13:1076445, 2023.
- [24] Yulia I Loktionova, Evgeny A Zherebtsov, Elena V Zharkikh, Igor O Kozlov, Angelina I Zherebtsova, Victor V Sidorov, Sergei G Sokolovski, Ilya E Rafailov, Andrey V Dunaev, and Edik U Rafailov. Studies of age-related changes in blood perfusion coherence using wearable blood perfusion sensor system. In *European Conference on Biomedical Optics*, page 11075\_6. Optica Publishing Group, 2019.
- [25] Elena Zharkikh, Viktor Dremin, Evgeny Zherebtsov, Andrey Dunaev, and Igor Meglinski. Biophotonics methods for functional monitoring of complications of diabetes mellitus. *Journal of biophotonics*, 13(10):e202000203, 2020.
- [26] Evgeny A Zherebtsov, Elena V Zharkikh, Igor O Kozlov, Yulia I Loktionova, Angelina I Zherebtsova, Ilya E Rafailov, Sergei G Sokolovski, Victor V Sidorov, Andrey V Dunaev, and Edik U Rafailov. Wearable sensor system for multipoint measurements of blood perfusion: pilot studies in patients with diabetes mellitus. In *European Conference on Biomedical Optics*, page 11079\_62. Optica Publishing Group, 2019.
- [27] Elena Zharkikh, Yulia Loktionova, V. Sidorov, Alexander Krupatkin, Galina Masalygina, and Andrey Dunaev. Control of blood microcirculation parameters in therapy with alpha-lipoic acid in patients with diabetes mellitus. *Human Physiology*, 48:456–464, 09 2022. doi: 10.1134/S0362119722040156.
- [28] Elena V Zharkikh, Yulia I Loktionova, Andrey A Fedorovich, Alexander Y Gorshkov, and Andrey V Dunaev. Assessment of blood microcirculation changes after covid-19 using wearable laser doppler flowmetry. *Diagnostics*, 13(5):920, 2023.
- [29] Batta Mahesh. Machine learning algorithms-a review. *International Journal of Science and Research (IJSR).[Internet]*, 9(1):381–386, 2020.
- [30] Trevor Hastie, Robert Tibshirani, Jerome H Friedman, and Jerome H Friedman. *The elements of statistical learning: data mining, inference, and prediction*, volume 2. Springer, 2009.
- [31] Scott M Lundberg and Su-In Lee. A unified approach to interpreting model predictions. *Advances in neural information processing systems*, 30, 2017.
- [32] World Health Organization et al. The impact of the covid-19 pandemic on noncommunicable disease resources and services: results of a rapid assessment. 2020.
- [33] Ruben D Restrepo, Melissa T Alvarez, Leonard D Wittnebel, Helen Sorenson, Richard Wettstein, David L Vines, Jennifer Sikkema-Ortiz, Donna D Gardner, and Robert L Wilkins. Medication adherence issues in patients treated for copd. *International journal of chronic obstructive pulmonary disease*, 3(3):371–384, 2008.

- [34] Zehra Yonel, Praveen Sharma, Asma Yahyouche, Zahraa Jalal, Thomas Dietrich, and Iain L Chapple. Patients' attendance patterns to different healthcare settings and perceptions of stakeholders regarding screening for chronic, non-communicable diseases in high street dental practices and community pharmacy: a cross-sectional study. *BMJ open*, 8(11):e024503, 2018.
- [35] Paulina Mularczyk-Tomczewska, Adam Żarnowski, Mariusz Gujski, Janusz Sytnik-Czetwertyński, Igor Pańkowski, Rafał Smoliński, and Mateusz Jankowski. Preventive health screening during the covid-19 pandemic: a cross-sectional survey among 102,928 internet users in poland. *Journal of Clinical Medicine*, 11(12):3423, 2022.
- [36] Andrea Bagnò and Romeo Martini. Wavelet analysis of the laser doppler signal to assess skin perfusion. In *2015 37th Annual International Conference of the IEEE Engineering in Medicine and Biology Society (EMBC)*, pages 7374–7377. IEEE, 2015.
- [37] Alexey Goltsov, Anastasia V Anisimova, Maria Zakharkina, Alexander I Krupatkin, Viktor V Sidorov, Sergei G Sokolovski, and Edik Rafailov. Bifurcation in blood oscillatory rhythms for patients with ischemic stroke: A small scale clinical trial using laser doppler flowmetry and computational modeling of vasomotion. *Frontiers in physiology*, 8:251012, 2017.
- [38] Angeina I. Zhrebtsova, Viktor V. Dremine, Irina Makovik, Evgeny A. Zhrebtsov, Andrey V. Dunaev, A. N. Goltsov, Sergei Sokolovski, and Edik U. Rafailov. Multimodal optical diagnostics of the microhaemodynamics in upper and lower limbs. *Frontiers in Physiology*, 10, 2019.
- [39] Evgeny Zhrebtsov, Elena Zharkikh, Yulia Loktionova, Angelina Zhrebtsova, Victor Sidorov, E.U. Rafailov, and Andrey Dunaev. Wireless dynamic light scattering sensors detect microvascular changes associated with ageing and diabetes. *IEEE transactions on bio-medical engineering*, 70:3073–3081, 05 2023.
- [40] Vera Ralevic, Abebech Belai, and Geoffrey Burnstock. Effects of streptozotocin-diabetes on sympathetic nerve, endothelial and smooth muscle function in the rat mesenteric arterial bed. *European journal of pharmacology*, 286(2):193–199, 1995.
- [41] Anne Humeau, Audrey Koïtka, Pierre Abraham, Jean-Louis Saumet, and Jean-Pierre L'Huillier. Spectral components of laser doppler flowmetry signals recorded in healthy and type 1 diabetic subjects at rest and during a local and progressive cutaneous pressure application: scalogram analyses. *Physics in Medicine & Biology*, 49(17):3957, 2004.
- [42] Yih-Kuen Jan, Sa Shen, Robert D Foreman, and William J Ennis. Skin blood flow response to locally applied mechanical and thermal stresses in the diabetic foot. *Microvascular research*, 89:40–46, 2013.
- [43] Yulia I Loktionova, Elena V Zharkikh, Igor O Kozlov, Evgeny A Zhrebtsov, Svetlana A Bryanskaya, Angelina I Zhrebtsova, Victor V Sidorov, Sergei G Sokolovski, Andrey V Dunaev, and Edik U Rafailov. Pilot studies of age-related changes in blood perfusion in two different types of skin. In *Saratov Fall Meeting 2018: Optical and Nano-Technologies for Biology and Medicine*, volume 11065, pages 184–188. SPIE, 2019.
- [44] Mou Saha, Viktor Dremine, Ilya Rafailov, Andrey Dunaev, Sergei Sokolovski, and Edik Rafailov. Wearable laser doppler flowmetry sensor: a feasibility study with smoker and non-smoker volunteers. *Biosensors*, 10(12):201, 2020.
- [45] Elena Zharkikh, Yulia Loktionova, Angelina Zhrebtsova, Mariia Tsyganova, Evgeny Zhrebtsov, and Alena Tiselko. Skin blood perfusion and fluorescence parameters in pregnant women with type 1 diabetes mellitus. pages 238–240, 10 2021.

# Contents

|          |   |           |
|----------|---|-----------|
| <b>1</b> | <b>Introduction</b>   | <b>1</b>  |
| 1.1      | Motivation . . . . .  | 1         |
| 1.2      | Literature Review . . . . .                                     | 3         |
| 1.3      | Contribution . . . . .  | 3         |
| <b>2</b> | <b>Study Design and Dataset Description</b>                     | <b>4</b>  |
| <b>3</b> | <b>Machine Learning and Explainable Artificial Intelligence</b> | <b>5</b>  |
| 3.1      | Machine Learning Models for DAS Prediction . . . . .            | 5         |
| 3.2      | Explainable AI . . . . .  | 8         |
| <b>4</b> | <b>Experimental Results</b>                                     | <b>8</b>  |
| 4.1      | All Features with 80:20 Split . . . . .                         | 8         |
| 4.1.1    | Binary Classification . . . . .                                 | 8         |
| 4.1.2    | Multi-class Classification . . . . .                            | 8         |
| 4.1.3    | Feature Importance . . . . .                                    | 9         |
| 4.2      | All Features with Cross-Validation . . . . .                    | 9         |
| 4.2.1    | Binary Classification with LOPO . . . . .                       | 10        |
| 4.2.2    | Binary Classification with 5-folds . . . . .                    | 10        |
| 4.2.3    | Multi-class Classification with LOPO . . . . .                  | 11        |
| 4.2.4    | Multi-class Classification with 5-folds . . . . .               | 11        |
| 4.3      | Multimodal Sensor Features . . . . .                            | 12        |
| 4.3.1    | Binary Classification with LOPO . . . . .                       | 12        |
| 4.3.2    | Binary Classification with 5-folds . . . . .                    | 12        |
| 4.4      | Top-10 Important Features . . . . .                             | 12        |
| 4.4.1    | Binary Classification with LOPO . . . . .                       | 12        |
| 4.4.2    | Binary Classification with 5-folds . . . . .                    | 13        |
| 4.4.3    | Multi-class Classification with LOPO . . . . .                  | 13        |
| 4.4.4    | Multi-class Classification with 5-folds . . . . .               | 13        |
| 4.5      | Health Issue Explanation . . . . .                              | 14        |
| <b>5</b> | <b>Conclusion</b>   | <b>14</b> |
| <b>6</b> | <b>Acknowledgement</b>  | <b>15</b> |
| <b>A</b> | <b>Full Literature Review</b>                                   | <b>21</b> |
| <b>B</b> | <b>Detailed Study Design and Dataset Description</b>            | <b>25</b> |
| B.1      | Clinical Definition and Data collection . . . . .               | 25        |
| B.2      | Data Analysis . . . . .   | 25        |

|          |   |           |
|----------|---|-----------|
| <b>C</b> | <b>Details of Experimental Setup</b>                            | <b>29</b> |
| C.1      | Experimental Setup: Machine Learning Models . . . . .           | 29        |
| C.2      | Experimental Setup: Explainable AI . . . . .                    | 30        |
| <b>D</b> | <b>Training and Evaluation Metrics</b>                          | <b>31</b> |
| D.1      | Case study . . . . .  | 31        |
| D.2      | Data Split . . . . .  | 32        |
| D.2.1    | Random 80:20 Split . . . . .                                    | 32        |
| D.2.2    | Leave-one-patient-out (LOPO) . . . . .                          | 32        |
| D.2.3    | K-Folds . . . . .   | 32        |
| D.3      | Evaluation Metrics . . . . .                                    | 33        |
| <b>E</b> | <b>ROC Plots</b>  | <b>35</b> |
| E.1      | All Features with 80:20 Split (Binary Classification) . . . . . | 35        |
| E.2      | All Features with Cross-Validation . . . . .                    | 38        |
| E.2.1    | Binary classification: LOPO . . . . .                           | 38        |
| E.2.2    | Binary classification: K-folds . . . . .                        | 41        |
| E.3      | Using multimodal sensor features classification . . . . .       | 44        |
| E.3.1    | Binary classification: LOPO . . . . .                           | 44        |
| E.3.2    | Binary classification: K-folds . . . . .                        | 47        |
| E.4      | Using Top-10 important features classification . . . . .        | 50        |
| E.4.1    | Binary classification: LOPO . . . . .                           | 50        |
| E.4.2    | Binary classification: K-folds . . . . .                        | 53        |

## A Full Literature Review

Global health faces dual challenges from infectious diseases like COVID-19 and rising non-communicable diseases (NCDs). The World Health Organization (WHO) report highlights that the COVID-19 pandemic has caused significant disruptions in chronic disease services. Specifically, 53% of countries reported disruptions in hypertension treatment, 49% in diabetes care, 42% in cancer treatment, and 31% in cardiovascular emergency services. Additionally, over 50% of countries postponed public screening programs for breast and cervical cancer due to the reassignment of healthcare staff to COVID-19 duties and the cancellation of planned treatments [32–35]. The use of remote monitoring devices without intervention is crucial to aid patients and healthcare professionals in timely classification and treatment. These devices can continuously monitor vital health indicators, detect abnormalities early, and alleviate the burden on the healthcare system.

### **A promising new wearable technology:**

Fortunately, advancements in technology offer promising solutions. Professor E. Rafailov's research group at Aston University has made significant strides in developing LDF/FS wearable devices [21]. They developed the devices using VCSEs, which demonstrated signal responses comparable to conventional tabletop monitors through volunteer-based assessments. These devices use Laser Doppler Flowmetry (LDF) and fluorescence spectroscopy (FS) for non-invasive early detection of vascular complications in diabetes and other conditions. LDF assesses tissue perfusion, oxygen saturation, and blood volume by analyzing backscatter from red blood cells using near-infrared and infrared light. FS complements LDF by detecting metabolic activity changes and advanced glycation end-products (AGEs) accumulation in diabetes, which contributes to microvascular damage and inflammation.

### **Specific details of analyzing the microcirculation using LDF and wavelet transformation:**

Currently, several principal frequency bands are distinguished in microvascular oscillations, reflecting various regulatory mechanisms: endothelial 0.0095–0.02 Hz, neurogenic 0.02–0.06 Hz, myogenic 0.06–0.16 Hz, respiratory 0.16–0.4 Hz, and cardiac 0.4–1.6 Hz [36].

### **Additional capabilities of Fluorescence Spectroscopy (FS):**

Additionally, other structural proteins of capillary and skin membranes also exhibit fluorescence: pentosidine residues formed during collagen glycation. Pathogenic factors such as hyperglycemia and oxidative stress in diabetes lead to increased protein glycation and accumulation of advanced glycation end products (AGEs), affecting the properties of collagen with specific wavelengths of light. This can be used to study skin fluorescence related to AGE accumulation, which is associated with the accumulation of these substances.

Currently, there is a growing interest in wearable electronic diagnostic devices because daily monitoring of parameters promises a new quality of diagnosis. Recently, multimodal approaches have been actively developed, allowing clinicians to obtain in vivo values of physiological and biochemical parameters, as well as to comprehensively assess the viability of the subcutaneous microcirculatory system. One of the first developments of wearable devices for estimating subcutaneous microcirculatory tissue system (MTS) parameters is the "LAZMA PF" analyzer, produced by Aston Medical Technology Ltd., UK, under the name "FED-1B". This device integrates a multimodal approach, specifically including 2 channels for laser Doppler flowmetry (LDF) and fluorescence spectroscopy (FS), designed into a new device named MDFED-2B<sup>3</sup>.

This technology is renowned for its non-invasive measurement capabilities in living tissues. Studies have been conducted at various sites such as the wrist, ankle, thigh, and fingertips. It has many applications, including research on metabolic and vascular complications of diabetes, automatic cerebral vascular analysis, and monitoring cerebral circulation in both healthy individuals and those with disorders. It provides continuous, non-invasive monitoring during diagnostic, treatment, and post-treatment phases. Spectral characteristic changes have been observed in conditions such as malignant tumors, surgical trauma, increased arterial pressure, and many others. It is also used to assess the functional status of the cerebral vascular system in patients with acute and chronic cerebrovascular disorders.

---

<sup>3</sup><https://amedtech.co.uk/product/mfed-2b/>

Monte Carlo modeling has shown a penetration depth of up to 2 mm for the LDF channel (deep vessels) and 1 mm for the FS channel. Sensors can monitor parameters such as perfusion, movement, skin temperature, and metabolic activity, providing crucial information for evaluating various physiological processes.

**The technical details of the MDFED-2B wearable device and how it uses its two channels for LDF and FS measurements:** The two channels combined in the design characteristics of the wearable device are used for multimodal optical diagnostics. A distinctive feature of the wearable devices under consideration is the absence of optical fibers in the design, which reduces common motion artifacts on the fibers. The wearable devices are placed on the skin for direct irradiation from a window on the underside of the device, recording the emitted (secondary) radiation from the biological tissue on the back of the device and transmitting measurement data to a PC via Bluetooth or Wi-Fi protocol. The “MDFED-2B” wearable device with 2 optical diagnostic channels uses an 850 nm VCSEL chip as the single-mode laser source with 0.8 mW power in the LDF channel, directly transmitting radiation to the skin. In the FS channel, a UV 365 nm LED is used, with a pulse power of 1.4 mW and an average power of 0.35 mW to excite endogenous NADH fluorescence at wavelengths between 460-470 nm. The amplitude of NADH fluorescence intensity (ANADH) is normalized to backscattered radiation to reduce the influence of varying blood filling in the biological tissue, which arises, among other reasons, from artifacts related to different pressures on the skin surface. The distance between the windows of the 2 channels is approximately 1 cm (the distance between the radiation source and detector). The placement of wearable devices for MTS diagnostics of the human body and wireless connection to a personal computer or smartphone is shown on symmetric regions of the limbs. Common locations for wearable devices on the body’s biological tissue depend on the diagnostic task: these are usually symmetrical points on the right and left of the upper and lower limbs, areas with direct arterio-venous connections (hand or fingertip) and with predominant nutritional blood flow (forearm or lower leg), and on the forehead at the supraorbital artery regions.

**The applications of the LDF/FS technology in the MDFED-2B wearable device for various medical conditions:**

Studies have applied this technology to measurements in various patients. Low perfusion parameters were observed in 19 patients with acute ischemic stroke (AIS) in both the affected and unaffected hemispheres, and were lower in patients with chronic cerebrovascular disease [37]. It evaluated the severity of microcirculatory and metabolic disorders in 41 rheumatic diseases and 76 diabetes patients. Research on perfusion in patients with joint microcirculatory disorders in the hands [38]. Cardiovascular risk in diabetic and elderly patients. A study on three groups, including 37 diabetic patients, 37 elderly individuals, and 58 young individuals, comparing average perfusion using the LDF (Laser Doppler Flowmetry) method, showed that blood microcirculation index values increase with age and the progression of diabetes [39]. There was no statistically significant difference between patients and the older control group in average perfusion. However, the average energy of blood flow oscillations decreased in patients with diabetes in the endothelial, neurogenic, myogenic, and respiratory ranges. In terms of neurogenic and myogenic variability, statistically significant differences were found between the diabetic patient group and the older control group, reflecting the influence of sympathetic nervous distribution and vascular smooth muscle activity [40].

In another study, diabetic patients had significantly lower endothelial, neurogenic, and myogenic low-frequency oscillation values compared to healthy controls when measured near the head of the first metatarsal bone.[41] When measuring on smooth skin, Jan and colleagues also showed reduced neurogenic and myogenic regulation in diabetes in response to heat. According to the authors, such changes in blood flow regulation are due to disruptions in the autonomic component of the peripheral nervous system, causing blood flow to be diverted to shunts.

The most common characteristic of microcirculatory disorders related to diabetes is the dysfunction of smooth muscle, endothelial cells, and perivascular nerves in the periphery, which explains the decrease in low-frequency perfusion oscillation values [39]. A study on an animal model of diabetes also showed that neurogenic distribution disorders in peripheral vessels are the primary factor contributing to microcirculatory dysfunction, leading to endothelial dysfunction and impaired smooth muscle function in the vascular system [42, 38, 26, 43]. Non-smokers had higher blood perfusion levels compared to smokers, while smokers exhibited greater variation in pulse frequency. These findings suggest that the LDF device is effective in detecting the cardiovascular impacts of smoking and could be useful for monitoring blood microcirculation and related pathologies in smokers. [44].

The device's advantages are its painlessness, quick results, no need for expensive consumables, and minimal impact on the patient.

**The validation steps taken before using the LDF/FS wearable devices (MDFED-2B) for various diagnoses:**

Before deploying these new wearable devices for various diagnostic tasks, their potential for multipoint perfusion measurement was investigated. These devices were used to analyze the synchronization of blood flow on the skin in analogous regions of opposite limbs, both at rest and during various functional tests (occlusion or breath-holding). Studies have shown high synchronization of blood flow rhythms in the opposite limbs of healthy volunteers. The compact and highly sensitive devices can be used even outside clinical settings. Furthermore, these wearable devices show high repeatability of measurements at rest and during physiological tests, enhancing the diagnostic value of the measurements.

**Findings from an initial study using the LDF/FS wearable devices to investigate blood microcirculation:**

A study using new wearable devices examined blood microcirculation across age groups. Older adults showed higher perfusion levels in the middle palm and dorsal forearm, due to thinner skin reducing laser scattering and increasing diagnostic volume. Younger individuals had higher wavelet parameters in blood perfusion oscillations. These findings can aid in developing MTS study protocols for patients with various pathologies. [24].

**How the LDF/FS wearable device was used in a study on diabetes and microcirculation:**

Research using wearable diagnostic devices in endocrinology assessed microcirculatory function in 19 diabetes (DM) type 2 patients and 37 healthy individuals across two age groups. Results showed different average perfusion levels between healthy volunteers of different ages and between younger healthy volunteers and DM patients. Notably, wrist and fingertip perfusion levels in healthy groups showed no significant difference. This pilot study demonstrated that wireless LDF wearable devices are convenient for point-of-care testing, recording age-specific perfusion changes and changes related to diabetes development[26].

**A study using the LDF/FS wearable device to monitor the effects of alpha-lipoic acid treatment on microcirculation in diabetic patients:**

Another promising use of these wearable devices in endocrinology is monitoring 10 diabetes patients therapy involving intravenous alpha-lipoic acid. Studies showed a decrease in microcirculatory and nutritional blood flow and an increase in shunt blood flow during treatment. After treatment, patients' parameters approximated control group values, particularly in the lower limbs, which are more affected by diabetic complications due to higher stress factors. These changes suggest positive effects of the therapy [27].

**A study using the LDF/FS wearable device to investigate the impact of pregestational type 1 diabetes on microcirculation in pregnant women at different stages:**

The study examined multimodal wearable diagnostic devices' impact on pregestational type 1 diabetes in pregnant women, showing glucose variability monitoring's role in assessing vascular function and oxidative status. Ten pregnant women (ages 32, 7-22 weeks gestation) and seven healthy women (age 32) were monitored using the "Libre Freestyle" system. Results indicated reduced microvascular activity in pregnant patients' legs and increased NADH fluorescence, suggesting tissue respiration decline [45].

**A study using wearable LDF devices to analyze blood flow patterns in patients with COVID-19 during different stages of recovery:**

The study demonstrated the use of peripheral blood flow oscillation analysis with wearable LDF devices to diagnose vascular disorders in a COVID-19 patient during early and progressive recovery stages. Results showed a significant increase in neurogenic oscillation amplitude in the upper limbs, potentially leading to arteriolar and venular dilation and microcirculatory blood flow shunting, adversely affecting oxygen delivery and tissue metabolism. Wavelet analysis confirmed changes in average perfusion levels due to blood flow fluctuations, influenced by disease severity and specifics [28].

### **The potential the wearable LDF/FS devices in medical diagnosis:**

Summarizing all the given data, the presented wearable diagnostic devices with 2 optical channels for LDF and FS are a promising approach for evaluating the functional state of MTS. The multimodal approach of using LDF and FS makes it possible to simultaneously obtain physiological and metabolic information, which helps to comprehensively assess the state of the microcirculatory system. The results presented in studies demonstrated the possibility of using wearable devices to obtain objective information on MTS status under normal and pathological conditions. However, more detailed studies with larger patient cohorts and extended analysis of physiological conditions should be conducted for further clinical implementation.

One of the crucial tasks is to investigate the effects of various treatment protocols and lifestyle changes on microcirculatory and metabolic parameters using these wearable devices. Another important direction is developing machine learning algorithms for automated data analysis and interpretation, which could significantly enhance the diagnostic capabilities of wearable devices.

The development and application of wearable diagnostic devices with LDF and FS channels represent a significant advancement in medical diagnostics, offering non-invasive, real-time monitoring of the microcirculatory system and metabolic state. These devices hold great potential for improving patient care, particularly in managing chronic diseases and monitoring treatment efficacy. Our research aims to leverage this technology to build a dataset for stress detection. The volunteers in our work have diverse medical histories, including migraine, diabetes, STEMI, and hypertension. By exploring cutaneous blood microcirculation parameters using a non-invasive wearable device equipped with LDF and FS channels, we can gain valuable insights. To the best of our knowledge, our work pioneers in publishing a large LDF/FS wearable device dataset for mental health assessment.



## B Detailed Study Design and Dataset Description

### B.1 Clinical Definition and Data collection

The criteria of this study are described as follows:

- This study focuses on volunteers aged 18 and above.
- Volunteers must not have any medical conditions related to dermatological diseases on both hands and middle fingers.
- A total of 132 volunteers, aged 18 and above, of all genders, various occupations, and different ages, who are healthy and alert, were included.

Table 17 shows the depression, anxiety and stress scale (DAS21) questionnaire responses which we gave to our volunteers.

### B.2 Data Analysis

Our dataset focuses on understanding the factors influencing depression, anxiety, and stress (DAS) levels. To achieve this, we have collected and integrated data from three key sources: personal information, wearable sensor readings, and the DAS-21 questionnaire. This diverse data representation allows us to create a comprehensive picture of each individual's background, psychological state, and physiological responses.

Similar to a medical record, the dataset includes essential demographic details for each participant. Our research involved a wide range of ages (18-94) with an average participant age of 40. We also ensured participant diversity by including a variety of races (Asian, White, African) and genders (55.2% male, 44.5% female), as shown in Fig. 5a and Fig. 5b, respectively.

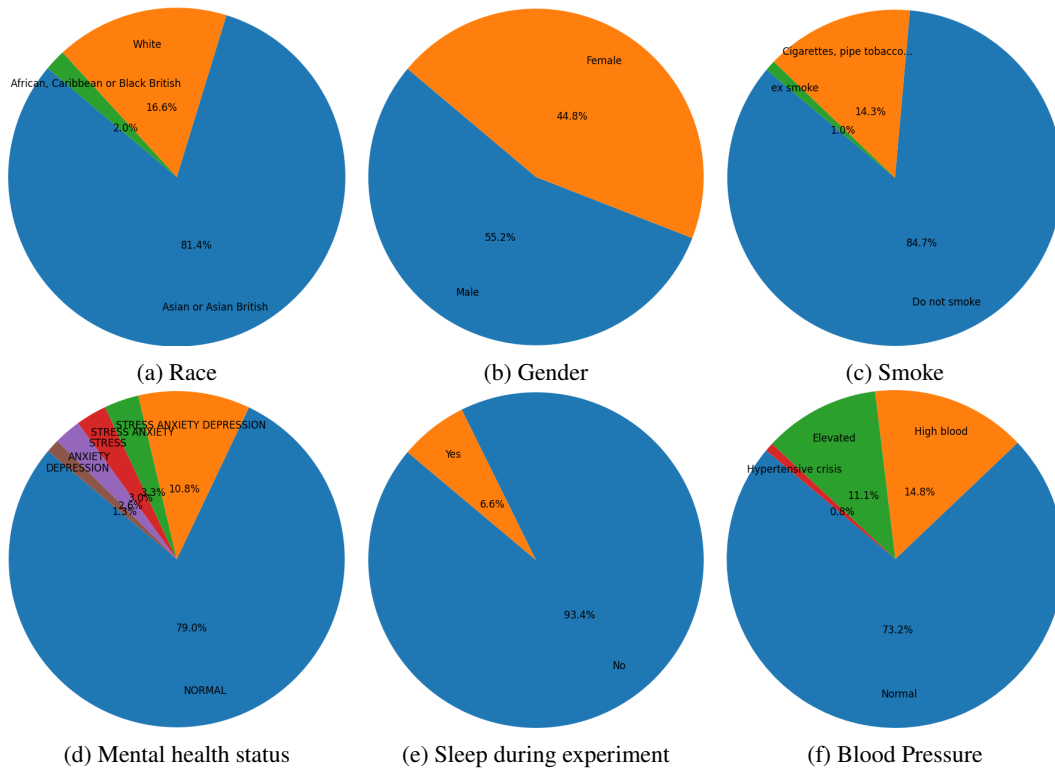


Figure 5: Data Analysis

In addition to the demographic information, we also investigate the effect of patients' routines and medical history, which is used to further understand potential contributors to DAS. As shown in Fig

Table 17: Depression, anxiety and stress scale (DAS21) questionnaire responses.

| No.    | Question  | 0 | 1 | 2 | 3 |
|--------|---|---|---|---|---|
| 1 (s)  | I found it hard to wind down  | 0 | 1 | 2 | 3 |
| 2 (a)  | I was aware of dryness of my mouth  | 0 | 1 | 2 | 3 |
| 3 (d)  | I couldn't seem to experience any positive feeling at all   | 0 | 1 | 2 | 3 |
| 4 (a)  | I experienced breathing difficulty (e.g. excessively rapid breathing, breathlessness in the absence of physical exertion)           | 0 | 1 | 2 | 3 |
| 5 (d)  | I found it difficult to work up the initiative to do things   | 0 | 1 | 2 | 3 |
| 6 (s)  | I tended to over-react to situations  | 0 | 1 | 2 | 3 |
| 7 (a)  | I experienced trembling (e.g. in the hands)   | 0 | 1 | 2 | 3 |
| 8 (s)  | I felt that I was using a lot of nervous energy   | 0 | 1 | 2 | 3 |
| 9 (a)  | I was worried about situations in which I might panic and make a fool of myself   | 0 | 1 | 2 | 3 |
| 10 (d) | I felt that I had nothing to look forward to  | 0 | 1 | 2 | 3 |
| 11 (s) | I found myself getting agitated   | 0 | 1 | 2 | 3 |
| 12 (s) | I found it difficult to relax   | 0 | 1 | 2 | 3 |
| 13 (d) | I felt down-hearted and blue  | 0 | 1 | 2 | 3 |
| 14 (s) | I was intolerant of anything that kept me from getting on with what I was doing   | 0 | 1 | 2 | 3 |
| 15 (a) | I felt I was close to panic   | 0 | 1 | 2 | 3 |
| 16 (d) | I was unable to become enthusiastic about anything  | 0 | 1 | 2 | 3 |
| 17 (d) | I felt I wasn't worth much as a person  | 0 | 1 | 2 | 3 |
| 18 (s) | I felt that I was rather touchy   | 0 | 1 | 2 | 3 |
| 19 (a) | I was aware of the action of my heart in the absence of physical exertion (e.g. sense of heart rate increase, heart missing a beat) | 0 | 1 | 2 | 3 |
| 20 (a) | I felt scared without any good reason   | 0 | 1 | 2 | 3 |
| 21 (d) | I felt that life was meaningless  | 0 | 1 | 2 | 3 |

5c, most of the participants do not smoke cigarettes, and the rate of people used to smoke is small compared to smoked people and non-smoke people. A similar observation is seen in the health issues attribute, in which the percentage of people who have problems with health issues is significantly smaller than normal people, as illustrated in Fig. 5d.

The dataset incorporates data collected from wearable devices worn by participants. As shown in Fig. 5e, we even recorded details like sleep patterns (sleeping vs. awake) and the hand used for blood sample collection during the study. These devices continuously monitor various physiological and activity-related aspects, providing real-time health information. Examples of data collected include Body Mass Index (BMI), heart rate, and Blood Pressure. Each data point is linked to a specific time, which allows us to analyze trends and potential correlations between a participant's physiological responses and their mental state over time. The experiment duration is around 15 minutes, at the end of the experiment.

Table 18: Blood perfusion ( $M^*$ ) with standard deviation and Maximum amplitude with standard deviation of the endothelial (A-E), neurogenic (A-N), myogenic (A-M), breath (A-R) and pulse (A-C) mechanism for Wellbeing vs Non-wellbeing, \*,  $p < 0.01$ , Mann-Whitney U test.

| Subgroup      | M_mean         | p-value  | A-E_mean      | p-value  | A-N_mean      | p-value | A-M_mean      | p-value  | A-R_mean      | p-value | A-C_mean      | p-value |
|---------------|----------------|----------|---------------|----------|---------------|---------|---------------|----------|---------------|---------|---------------|---------|
| All           | 22.54          |          | 1.49          |          | 1.46          |         | 1.17          |          | 0.7           |         | 0.93          |         |
|               | (4.73 - 37.23) |          | (0.34 - 3.36) |          | (0.33 - 3)    |         | (0.31 - 2.4)  |          | (0.22 - 1.29) |         | (0.39 - 1.68) |         |
| Wellbeing     | 21.02          | 0.016121 | 1.44          | 0.171585 | 1.4           | 0.27169 | 1.11          | 0.123042 | 0.66          | 0.0614  | 0.89          | 0.06069 |
|               | (4.73 - 35.59) |          | (0.34 - 3.42) |          | (0.31 - 2.99) |         | (0.29 - 2.35) |          | (0.2 - 1.18)  |         | (0.31 - 1.74) |         |
| Non-Wellbeing | 26.49          |          | 1.62          |          | 1.61          |         | 1.33          |          | 0.81          |         | 1.02          |         |
|               | (8.59 - 36.71) |          | (0.64 - 2.7)  |          | (0.49 - 2.96) |         | (0.5 - 2.32)  |          | (0.47 - 1.44) |         | (0.58 - 1.61) |         |

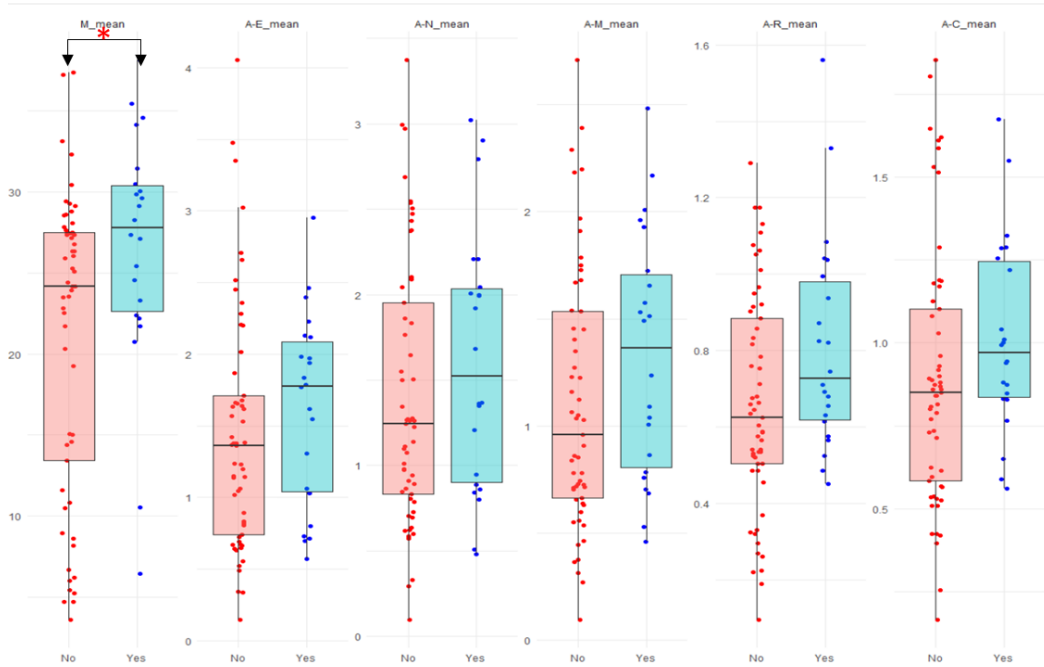


Figure 6: Blood perfusion ( $M^*$ ) with standard deviation and Maximum amplitude with a standard deviation of the endothelial (A-E), neurogenic (A-N), myogenic (A-M), breath (A-R) and pulse (A-C) mechanism for Wellbeing vs Non-wellbeing, \*,  $p < 0.01$ , Mann-Whitney U test.

Table 18 and Fig. 6 indicate that non-wellbeing individuals exhibit higher perfusion parameters and amplitude variations compared to wellbeing individuals. For the perfusion parameter  $M$ , wellbeing individuals have a mean value of 21.02 (95% CI, 4.73 - 35.59), whereas non-wellbeing individuals have a significantly higher  $M$  value of 26.49 (95% CI, 8.59 - 36.71), ( $p=0.016$ , Mann-Whitney U test). The endothelial, neural, muscle, respiratory, and cardiovascular amplitude variations all tend to be higher by more than 0.2, but the differences are not statistically significant.

As shown in Table 19 and Fig. 7, non-wellbeing individuals exhibit a statistically significant higher amplitude of perfusion parameter fluctuations ( $\delta$ ) compared to their wellbeing counterparts, with values of 4.79 (95% CI, 2.25 - 7.65) versus 3.64 (95% CI, 0.98 - 6.93), ( $p=0.007$ , Mann-Whitney

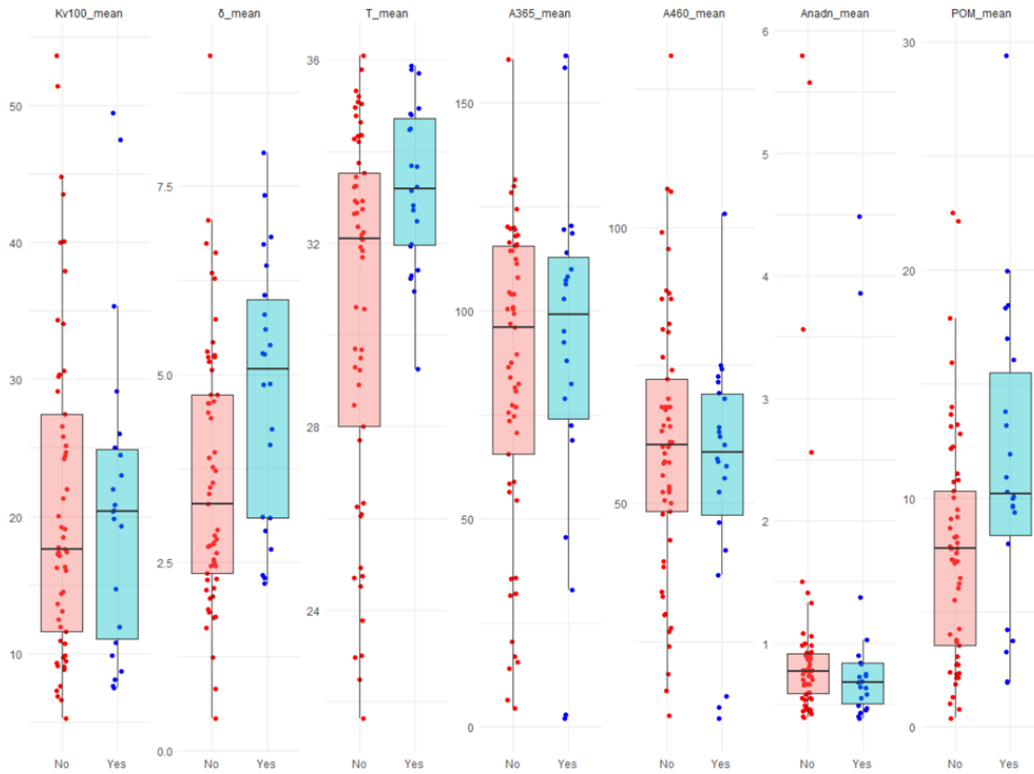


Figure 7: The parameters with standard deviation for Wellbeing vs Non-wellbeing: Kv100,  $\delta^*$ ,  $T^*$ , A365, A460, Anadn, POM\*, F-E; F-N; F-M; F-R; F-C, \*,  $p < 0.01$ , Mann-Whitney U test.

U test). Additionally, they have a significantly higher temperature at the measurement site, 33.21 (95% CI, 30.14 - 35.82) compared to 30.65 (95% CI, 22.68 - 35.6), ( $p=0.01$ , Mann-Whitney U test). Moreover, the metabolic index (POM) at the measurement site is also significantly elevated in non-wellbeing individuals, with values of 11.42 (95% CI, 1.95 - 24.42) versus 7.7 (95% CI, 0.85 - 20.43), ( $p=0.01$ , Mann-Whitney U test).

Table 19: The parameters with standard deviation for Wellbeing vs Non-wellbeing: Kv100,  $\delta^*$ ,  $T^*$ , A365, A460, Anadn, POM\*, F-E; F-N; F-M; F-R; F-C, \*,  $p < 0.01$ , Mann-Whitney U test.

| Subgroup      | Kv100_mean     | $\delta$ _mean | p-value  | T_mean          | p-value  | A365_mean       | A460_mean        | Anadn_mean    | POM_mean       | p-value  |
|---------------|----------------|----------------|----------|-----------------|----------|-----------------|------------------|---------------|----------------|----------|
| All           | 21.09          | 3.96           |          | 31.36           |          | 86.82           | 59.3             | 1.01          | 8.74           |          |
|               | (6.86 - 49.55) | (1.21 - 7.41)  |          | (22.95 - 35.79) |          | (4.42 - 158.6)  | (12.92 - 106.52) | (0.4 - 4.54)  | (0.99 - 22.15) |          |
| Wellbeing     | 21.12          | 3.64           | 0.007252 | 30.65           | 0.018427 | 85.43           | 60.64            | 1.01          | 7.7            | 0.010656 |
|               | (6.71 - 48.75) | (0.98 - 6.93)  |          | (22.68 - 35.6)  |          | (9.5 - 130.9)   | (17.2 - 106.8)   | (0.41 - 4.77) | (0.85 - 20.43) |          |
| Non-Wellbeing | 21             | 4.79           |          | 33.21           |          | 90.43           | 55.81            | 1             | 11.42          |          |
|               | (7.56 - 48.44) | (2.25 - 7.65)  |          | (30.14 - 35.82) |          | (2.52 - 159.81) | (12.05 - 88.06)  | (0.39 - 4.16) | (1.95 - 24.42) |          |

## C Details of Experimental Setup

This Appendix Section details the machine learning models employed for predicting depression, anxiety, and stress (DAS) levels, along with the Explainable Artificial Intelligence (XAI) technique used to interpret their decision-making processes.

### C.1 Experimental Setup: Machine Learning Models

To identify the most effective approach for predicting Depression, Anxiety, and stress (DAS) levels, we explored various machine learning algorithms. These algorithms leverage the collected wearable device data and DAS-21 questionnaire scores to estimate a patient's mental issues.

**Support Vector Machine (SVM)** is a well-established method that is known for its ability to effectively handle high-dimensional datasets, even with a relatively small sample size. SVMs aim to find a hyperplane in the feature space that maximizes the margin between different classes. In SVM, new data points are then classified based on which side of the hyperplane they fall on. SVMs are powerful for classification tasks with high-dimensional data, such as ours with potentially many features extracted from wearable sensors. They are effective even with limited data and offer good generalization capabilities. However, SVMs can be computationally expensive for very large datasets and may be less interpretable than other algorithms on this list.

**Random Forest Classifier** is an ensemble learning algorithm that combines the predictions of multiple, independently trained decision trees. Each tree is built using a random subset of features and data points, promoting diversity within the ensemble. The final prediction is made by majority vote or averaging the individual tree predictions. The algorithms are robust to overfitting due to their inherent diversity. They can handle various data types and perform well even with missing values. This approach is particularly useful for datasets with potential noise or inconsistencies.

**Gradient Boosting Classifier** is an algorithm that works by iteratively building an ensemble of weak decision trees. Each tree learns from the errors of the previous one, ultimately leading to a more robust and accurate model. Gradient boosting is known for its flexibility and ability to handle various data types, making it a strong contender for our analysis.

Building upon gradient boosting, **CatBoost** specifically addresses challenges in healthcare data. It incorporates advanced techniques for handling categorical features, such as one-hot encoding or custom loss functions, which can be problematic for traditional gradient boosting. Additionally, CatBoost prioritizes model interpretability by providing feature importance scores and visualizations of decision boundaries. CatBoost excels in scenarios with a high volume of categorical features, common in healthcare data. It offers improved interpretability compared to standard gradient boosting, allowing us to understand the factors influencing model predictions.

**LightGBM** (Light Gradient Boosting Machine) is a highly efficient implementation of the gradient boosting algorithm specifically designed for speed and performance. It utilizes techniques similar to gradient-based one-side sampling and feature importance sampling to focus on informative data points and reduce computational costs. LightGBM offers exceptional speed and accuracy, making it a compelling choice for large datasets. It is particularly efficient for memory usage, allowing for training in resource-constrained environments. LightGBM excels at handling large and complex datasets, making it suitable for our analysis where we have a high volume of data points from wearable devices.

In addition to the machine learning algorithms above, we also implemented a **Multi-layer Perceptron (MLP)** for health issue prediction. Unlike simpler models, MLPs excel at identifying complex, non-linear relationships within the data. This capability could be particularly valuable for uncovering subtle patterns between physiological signals and mental health states. The MLP neural network has two hidden layers and a final output layer with a unit. The network employs layer normalization, ReLU activation for hidden layers, and dropout to prevent overfitting. Finally, a sigmoid or a softmax activation function is applied to the output layer to transform the final values to the probability of classes.

By evaluating the performance of these diverse algorithms, we aim to identify the one that best predicts DAS levels in the context of our specific dataset and research goals.

## C.2 Experimental Setup: Explainable AI

In healthcare applications, ensuring trustworthy AI requires models to be not only accurate but also interpretable. Understanding the reasoning behind a model's predictions for DAS levels is crucial for building trust and confidence in its outputs. This empowers healthcare professionals and researchers to make informed decisions based on the predicted DAS levels and the underlying factors influencing those predictions. In this study, we leverage SHAP (Shapley Additive Explanations) to achieve interpretability and gain insights into the model's decision-making process for DAS prediction [31].

SHAP, a powerful approach for achieving interpretability, assigns an attribution value (SHAP value) to each feature for a given DAS prediction. This value represents the contribution of that specific feature (e.g., a specific physiological sensor reading or a DAS-21 questionnaire response) to the model's final prediction. High positive SHAP values indicate that the feature has a strong positive influence on the predicted DAS level (potentially indicating a higher likelihood of depression, anxiety, or stress). Conversely, low negative SHAP values signify a negative influence (potentially indicating a lower likelihood). By analyzing the SHAP values for each feature, we can gain insights into the relative importance of various factors shaping the model's predictions about a user's mental state.

This interpretability allows us to answer several key questions:

- Identification of key physiological and psychological indicators: What are the features from wearable sensor data and questionnaire scores of a patient that have the most significant influence on the model's predictions? Understanding these can pinpoint crucial physiological and psychological indicators associated with DAS levels. This knowledge can inform the development of targeted interventions and preventative measures for mental health.
- Validation of model fairness and mitigation of bias: Are the model's predictions fair across different demographics (age, gender, etc.)? Examining SHAP values across these groups helps ensure that the model is not unfairly biased towards certain populations. This is crucial in healthcare applications where fairness and unbiased decision-making are paramount.
- Enhanced model transparency and trust: How does the model arrive at its predictions? By explaining the rationale behind the model's predictions through SHAP values, we can foster trust and confidence in its use among healthcare professionals and researchers. This transparency is essential for the adoption and responsible use of AI in mental health assessments.

## D Training and Evaluation Metrics

### D.1 Case study

Our study employs two primary approaches to train machine learning models for predicting DAS levels: binary classification and multi-class classification, as shown in Table 20 and Table 21. Both approaches leverage data from the DAS-21 questionnaire alongside potentially other features from the collected dataset. In addition, we consider three cases to investigate the models’ performances: Using all collected features as shown in Table 20, using only features extracted from wearable devices, and using top-10 important features as illustrated in Table 21.

Table 20: Model investigation with all collected features, in which we trained models with different data split methods: 80:20, 5-fold, and leave one patient out (LOPO). In addition, "x" presents the cases that are being trained in our investigation.

| Model             | All Features |             |                   |             |        |             |
|-------------------|--------------|-------------|-------------------|-------------|--------|-------------|
|                   | Split 80:20  |             | 5-Fold Validation |             | LOPO   |             |
|                   | Binary       | Multi-class | Binary            | Multi-class | Binary | Multi-class |
| Gradient Boosting | x            | x           | x                 | x           | x      | x           |
| Catboost          | x            | x           | x                 | x           | x      | x           |
| LightGBM          | x            | x           | x                 | x           | x      | x           |
| SVM               | x            | x           | x                 | x           | x      | x           |
| Random Forest     | x            | x           | x                 | x           | x      | x           |
| MLP               | x            |             |                   |             |        |             |

Table 21: Model investigation with sensor features and top-10 important features. We trained the models with various data split methods: 80/20 train-test split, 5-fold cross-validation, and LOPO cross-validation. The "x" marks in the table indicate the specific model-data combinations investigated in this study.

| Model              | Sensor Features   |             |        |             | Top-10 Important Features |             |        |             |
|--------------------|-------------------|-------------|--------|-------------|---------------------------|-------------|--------|-------------|
|                    | 5-Fold Validation |             | LOPO   |             | 5-Fold Validation         |             | LOPO   |             |
|                    | Binary            | Multi-class | Binary | Multi-class | Binary                    | Multi-class | Binary | Multi-class |
| mGradient Boosting | x                 | x           | x      | x           | x                         | x           | x      | x           |
| Catboost           | x                 | x           | x      | x           | x                         | x           | x      | x           |
| LightGBM           | x                 | x           | x      | x           | x                         | x           | x      | x           |
| SVM                | x                 | x           | x      | x           | x                         | x           | x      | x           |
| Random Forest      | x                 | x           | x      | x           | x                         | x           | x      | x           |
| MLP                | x                 | x           | x      | x           |                           |             |        |             |

For binary classification, this approach simplifies the prediction task by transforming the DAS levels into a binary classification problem. In particular, we utilize the information from the DAS-21 questionnaire as labels, focusing on the mental health state of the participants. We categorize participants into two classes based on their DAS-21 scores:

- Normal: This class comprises participants who score within the normal range for depression, anxiety, and stress according to established DAS-21 scoring guidelines.
- Abnormal: This class encompasses participants whose DAS-21 scores indicate potential symptoms of depression, anxiety, or stress.

By converting the problem into a binary classification task, we can train models to distinguish between individuals with normal mental health states and those with potential mental health concerns based on their DAS-21 responses and potentially other features from the dataset.

For multi-class classification, this approach aims for a more granular prediction by treating DAS levels as a multi-class classification problem. Instead of collapsing mental health states into two categories, we define multiple classes based on the established DAS-21 scoring ranges: Normal, stress, stress Anxiety, and stress anxiety depression.

## D.2 Data Split

### D.2.1 Random 80:20 Split

In machine learning, dividing the dataset into training and testing subsets is crucial for evaluating model performance. One common approach is the random 80:20 split, where 80% of the randomly-shuffled data is used for training the model, and the remaining 20% is reserved for testing. This method is favored for its balance between providing enough data for the model to learn effectively and retaining a significant portion for unbiased performance evaluation.

```
from sklearn.model_selection import train_test_split

# Assuming `X` is the feature matrix and `y` is the target vector
X_train, X_test, y_train, y_test = train_test_split(X, y, test_size=0.2
                                                    , random_state=42)
```

### D.2.2 Leave-one-patient-out (LOPO)

Predictive models for diagnosis or treatment outcomes must generalize well across different patients. Leave-one-patient-out (LOPO) [30] ensures that the model is evaluated on its ability to perform on new patients not seen during training. For each iteration, all data points from one patient are used as the test set, while the data from all other patients are used to train the model. This process is repeated for each individual in the dataset, ensuring that every patient's data is used as a test set exactly once.

```
def leave_one_person_out(patient_ids):
    loo = dict()
    for patient_id in set(patient_ids):
        loo[patient_id] = None

    for patient_id in loo:
        train_indices, test_indices = [], []

        for i in range(len(patient_ids)):
            if patient_ids[i] == patient_id:
                test_indices.append(i)
            else:
                train_indices.append(i)

        loo[patient_id] = [train_indices, test_indices]

    return loo

patient_ids = list(df_rawdata['Patient_ID'])
loo = leave_one_person_out(patient_ids)

for patient_id in loo:
    # Leave one out
    train_indices = np.array(loo[patient_id][0])
    test_indices = np.array(loo[patient_id][1])

    X_train = X[train_indices]
    X_test = X[test_indices]
    y_train = y[train_indices]
    y_test = y[test_indices]
```

### D.2.3 K-Folds

K-fold cross-validation is a robust technique for training machine learning models in healthcare, ensuring reliable and unbiased performance evaluation [30]. K-fold cross-validation mitigates the risk of overfitting, maximizes data utilization, and enhances the model's generalizability, which is



crucial for accurately predicting patient outcomes and making informed medical decisions. It involves randomly partitioning the dataset into  $k$  equally sized folds, where the model is trained on  $k-1$  folds and validated on the remaining fold. This process is repeated  $k$  times, with each fold serving as the validation set once, and the performance metrics are averaged to provide a comprehensive assessment. Note that for each fold there is no patient overlapping. In the scope of this work, we used 5-fold cross-validation and 10 seeds for training, which means 5-fold was trained for 10 times to avoid varying results.

```
def k_fold(patient_ids, number_of_folds = 5):
    patient_id_dict = dict()
    for patient_id in set(patient_ids):
        patient_id_dict[patient_id] = []

    for i in range(len(patient_ids)):
        patient_id = patient_ids[i]
        patient_id_dict[patient_id].append(i)

    kfold_dict = dict()
    i, k = 0, len(patient_id_dict.keys()) // number_of_folds
    queue = list(patient_id_dict.keys())

    while queue:
        random.shuffle(queue)
        patient_id_test = [j for j in queue[0:k]]
        patient_id_train = [j for j in set(patient_id_dict.keys()) - set(
            patient_id_test)]

        train_indices, test_indices = [], []
        for patient_id in patient_id_train:
            train_indices += patient_id_dict[patient_id]
        for patient_id in patient_id_test:
            test_indices += patient_id_dict[patient_id]
        kfold_dict[i] = [train_indices, test_indices]

        queue = queue[k:]
        i += 1

    return kfold_dict

patient_ids = list(df_rawdata['Patient_ID'])

for seed in range(10):
    kfold = k_fold(patient_ids, number_of_folds=5)
    for k in kfold:
        # K-fold
        train_indices = np.array(kfold[k][0])
        test_indices = np.array(kfold[k][1])

        X_train = X[train_indices]
        X_test = X[test_indices]
        y_train = y[train_indices]
        y_test = y[test_indices]
```

### D.3 Evaluation Metrics

To assess the performance of the machine learning models for predicting Depression, Anxiety, and stress (DAS) levels, we employ two key evaluation metrics: Receiver Operating Characteristic (ROC) AUC (Area Under the Curve) and Precision-Recall (PR) AUC. These metrics provide a comprehensive assessment of the model's discriminative ability and its performance in handling class imbalances.

The ROC AUC metric measures the ability of the model to distinguish between classes. It plots the True Positive Rate (TPR) against the False Positive Rate (FPR) at various threshold settings. The AUC value ranges from 0 to 1, where a value of 1 indicates perfect classification and a value of 0.5 suggests performance no better than random guessing. A higher ROC AUC indicates that the model is better at differentiating between the positive and negative classes.

In our study, we calculate the ROC AUC to assess how well our model can predict DAS levels across the entire range of possible thresholds. This metric is particularly useful in healthcare applications, where the cost of false positives and false negatives can vary, and understanding the trade-offs between sensitivity and specificity is crucial.

While ROC AUC provides a good overall measure of performance, it can be insensitive to class imbalance. In our case, the prevalence of depression, anxiety, and stress might be lower than the prevalence of healthy individuals. The PR curve addresses this by plotting Precision against Recall.

## E ROC Plots

This section shows the ROC AUC and ROC PR plots for all binary classification results above.

### E.1 All Features with 80:20 Split (Binary Classification)

Figure 8, 9, 10, 11, 12, 13 shows the ROC AUC and ROC PR plots for all features binary classification models using Gradient Boosting, Catboost, LightGBM, SVM, Random Forest, and MLP respectively, with a random 80:20 split. These figures are plots from Table 3 in Section 4.1.

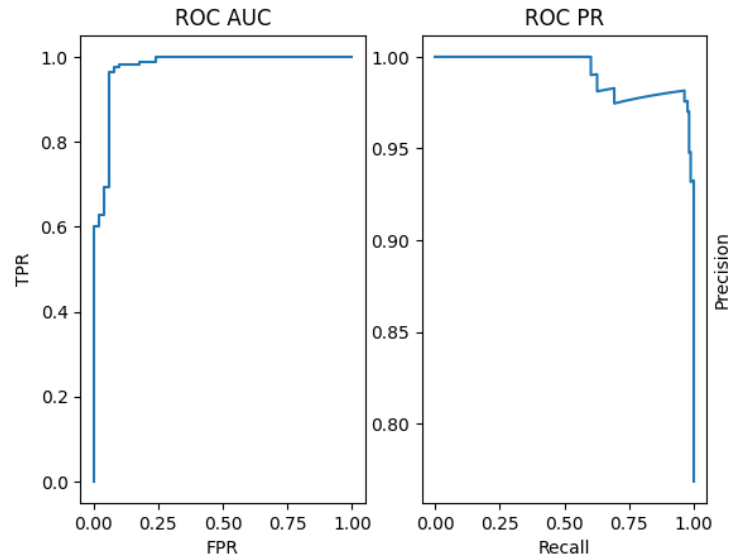


Figure 8: All features with 80:20 split, binary classification: Gradient Boosting

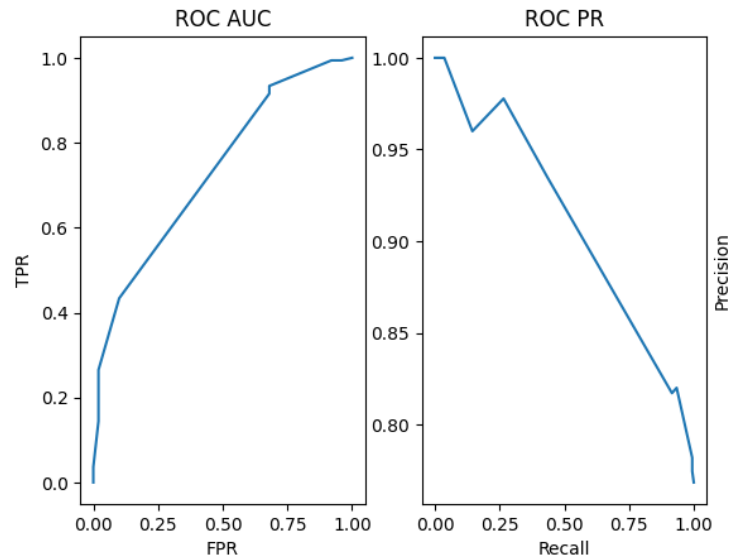


Figure 9: All features with 80:20 split, binary classification: Catboost

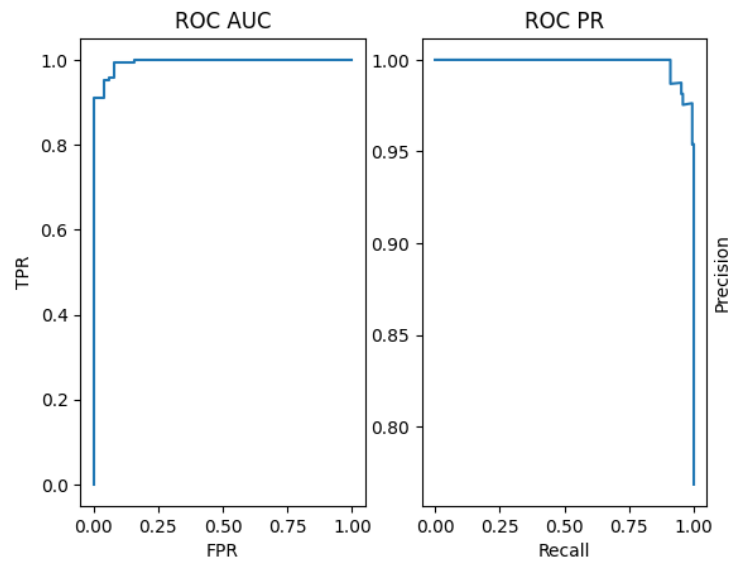


Figure 10: All features with 80:20 split, binary classification: LightGBM

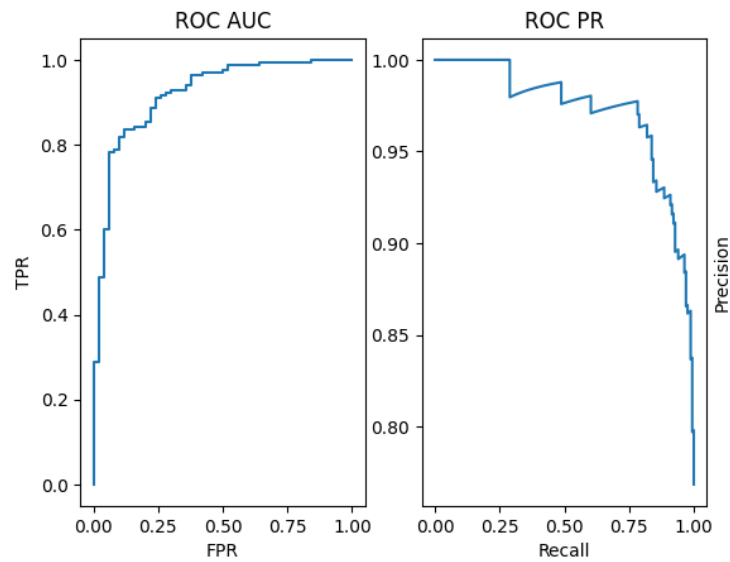


Figure 11: All features with 80:20 split, binary classification: SVM

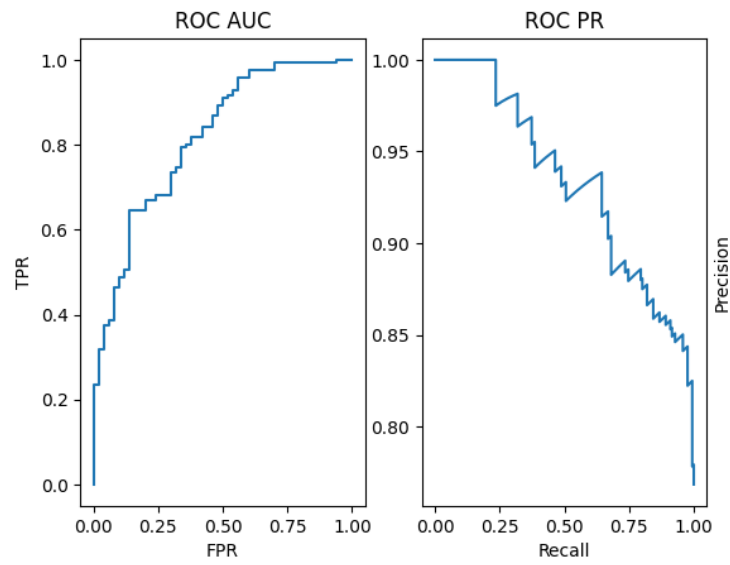


Figure 12: All features with 80:20 split, binary classification: Random forest

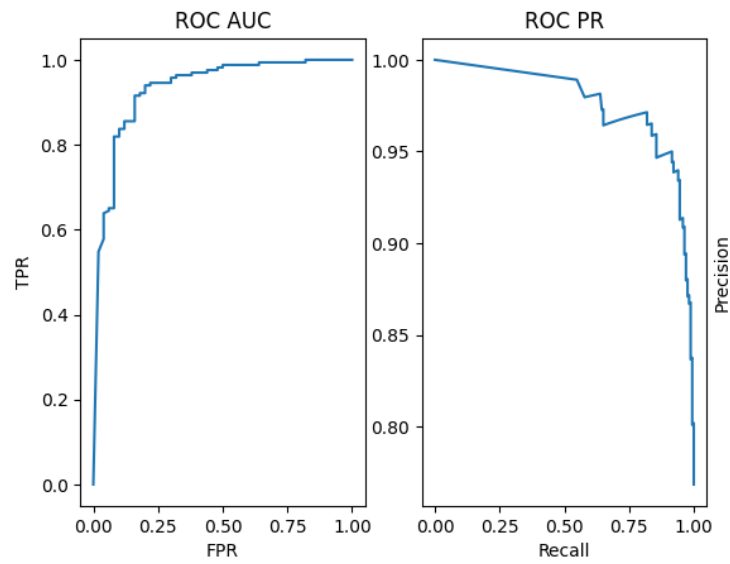


Figure 13: All features with 80:20 split, binary classification: MLP

## E.2 All Features with Cross-Validation

### E.2.1 Binary classification: LOPO

Figure 14, 15, 16, 17, 18, 19 shows the ROC AUC and ROC PR plots for all features binary classification models using Gradient Boosting, Catboost, LightGBM, SVM, Random Forest, and MLP respectively, with a LOPO split. These figures are plots from Table 7 in Section 4.2.

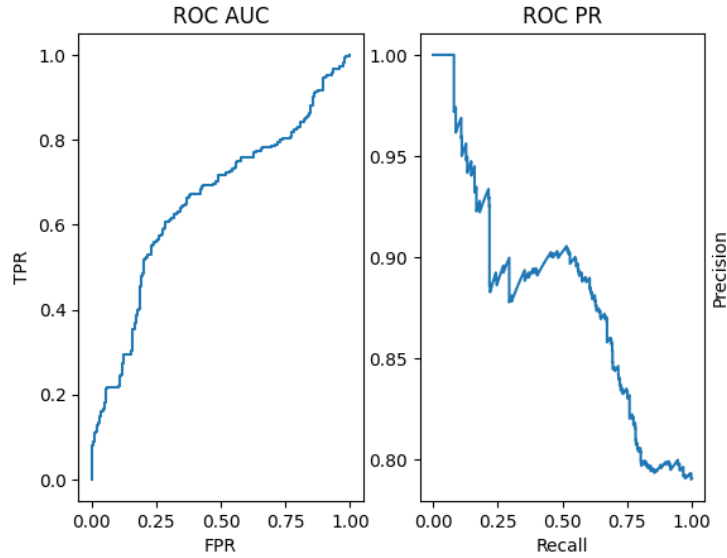


Figure 14: All features with LOPO, binary classification: Gradient Boosting

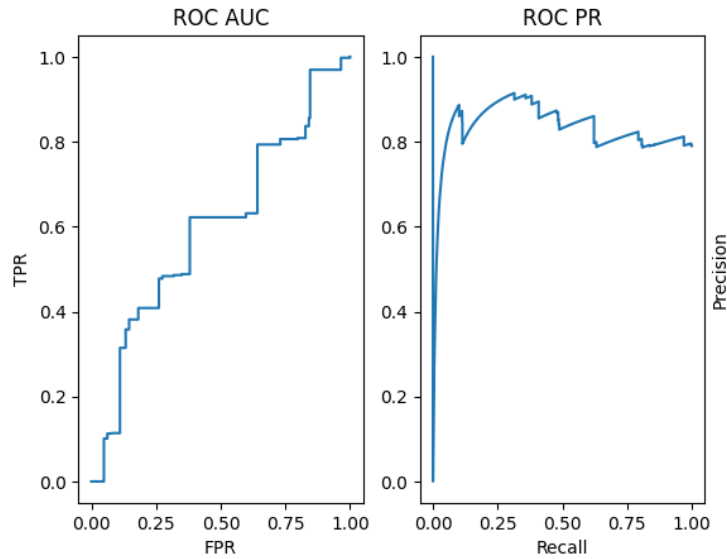


Figure 15: All features with LOPO, binary classification: Catboost

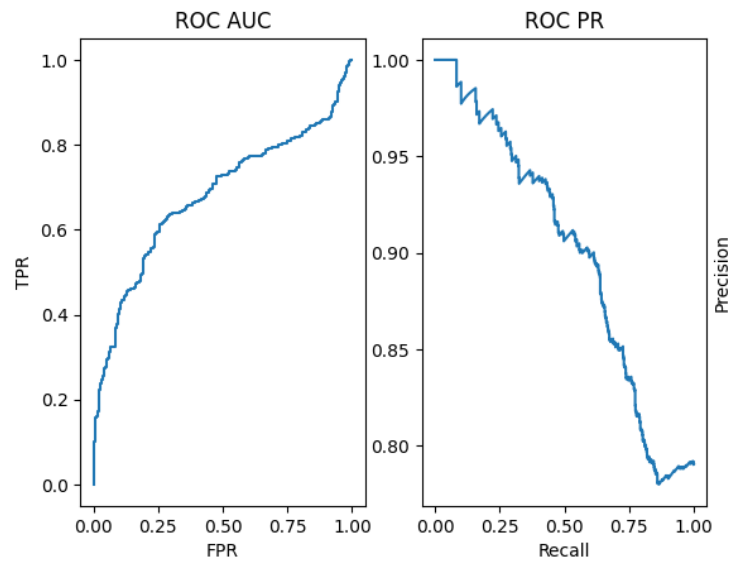


Figure 16: All features with LOPO, binary classification: LightGBM

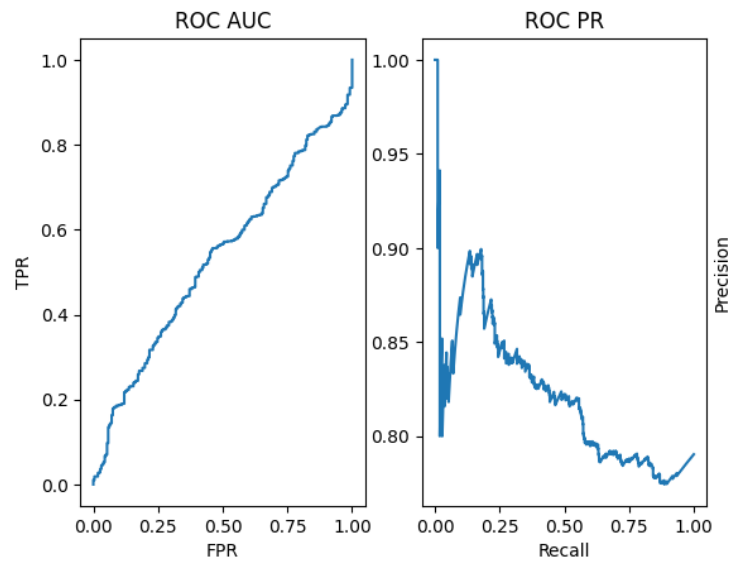


Figure 17: All features with LOPO, binary classification: SVM

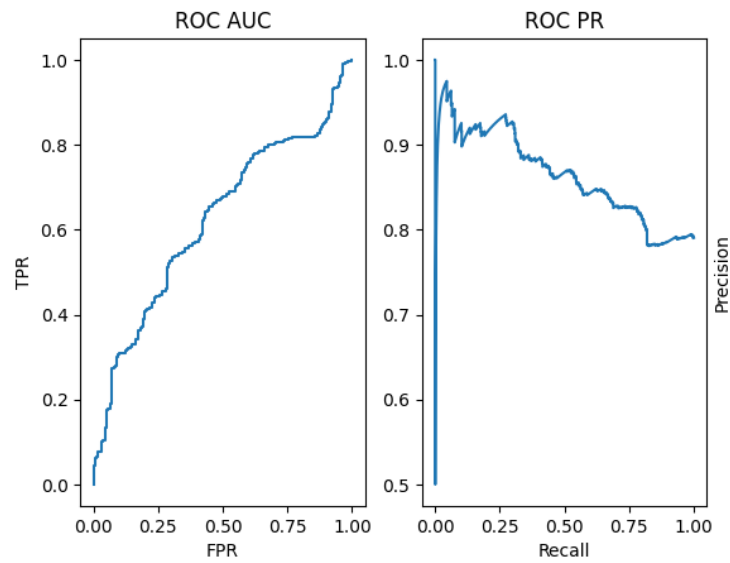


Figure 18: All features with LOPO, binary classification: Random Forest

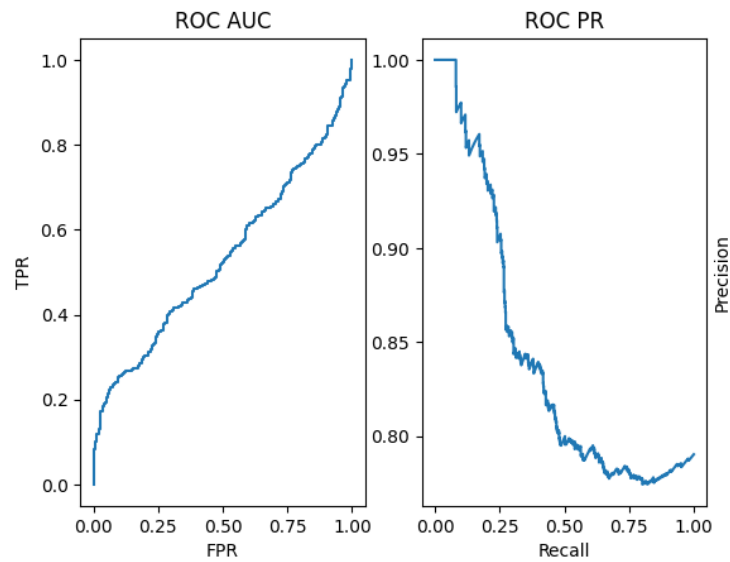


Figure 19: All features with LOPO, binary classification: MLP



### E.2.2 Binary classification: K-folds

Figure 20, 21, 22, 23, 24, 25 shows the ROC AUC and ROC PR plots for all features binary classification models using Gradient Boosting, Catboost, LightGBM, SVM, Random Forest, and MLP respectively, with a K-folds split. These figures are plots from Table 8 in Section 4.2.

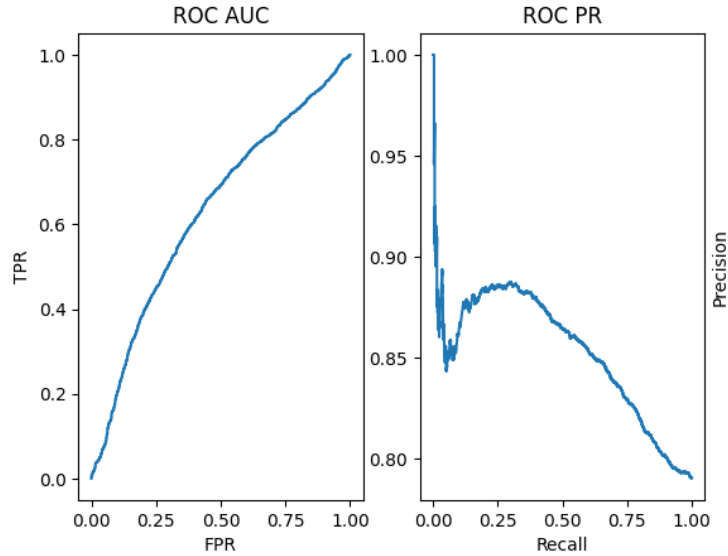


Figure 20: All features with K-folds, binary classification: Gradient Boosting

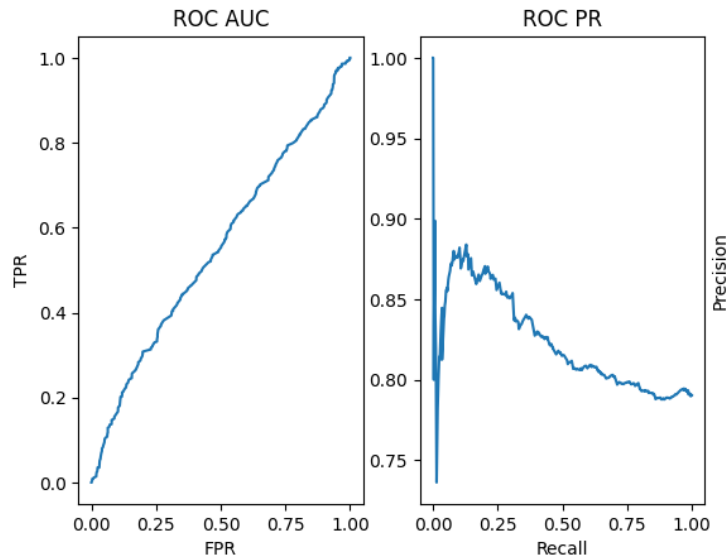


Figure 21: All features with K-folds, binary classification: Catboost

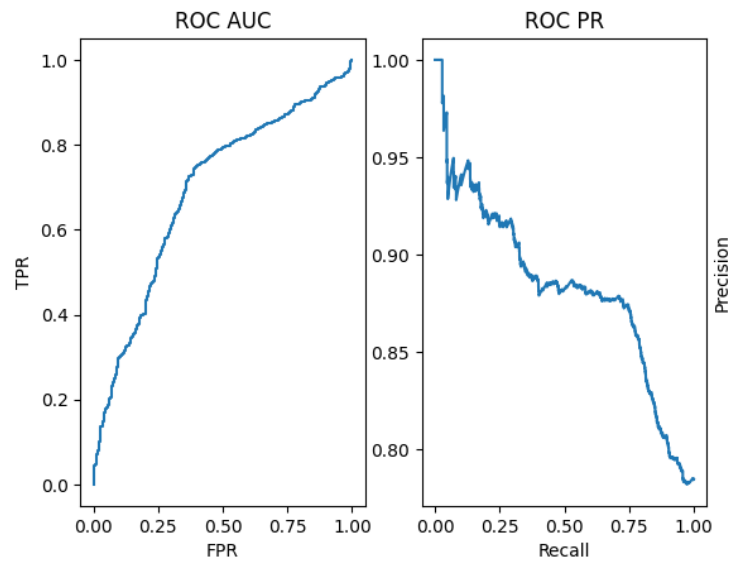


Figure 22: All features with K-folds, binary classification: LightGBM

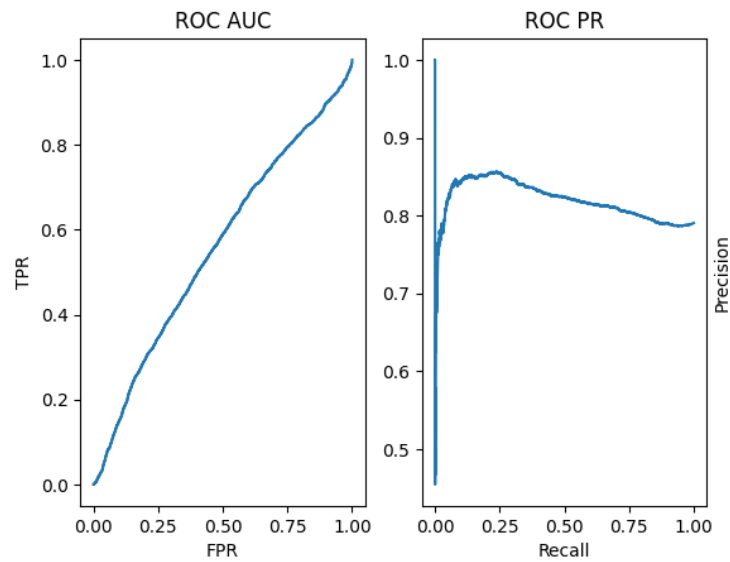


Figure 23: All features with K-folds, binary classification: SVM

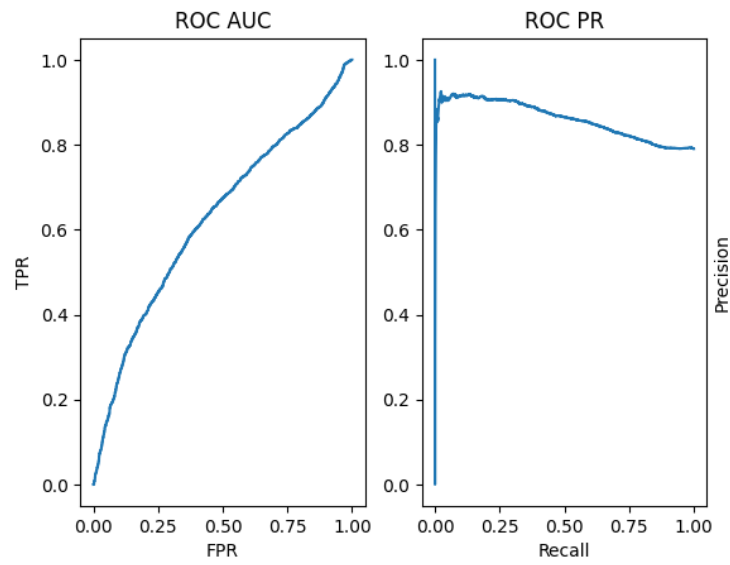


Figure 24: All features with K-folds, binary classification: Random Forest

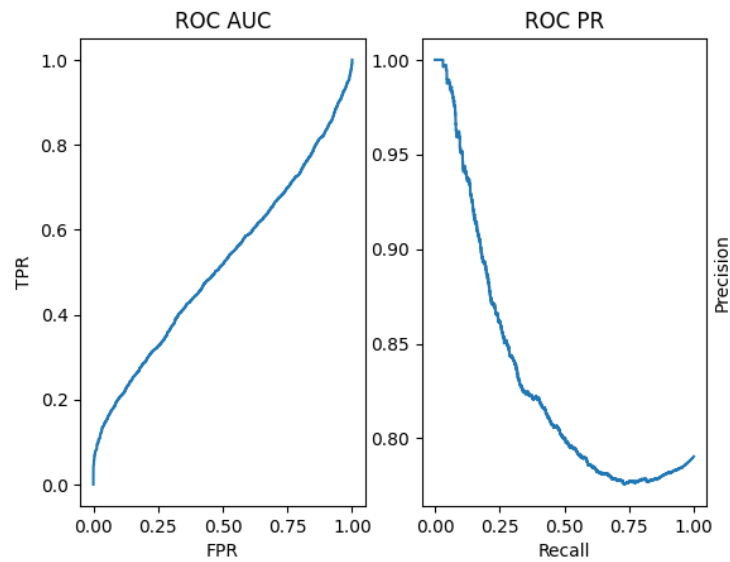


Figure 25: All features with K-folds, binary classification: MLP

### E.3 Using multimodal sensor features classification

#### E.3.1 Binary classification: LOPO

Figure 26, 27, 28, 29, 30, 31 shows the ROC AUC and ROC PR plots for multimodal sensor features binary classification models using Gradient Boosting, Catboost, LightGBM, SVM, Random Forest, and MLP respectively, with a LOPO split. These figures are plots from Table 11 in Section 4.3.

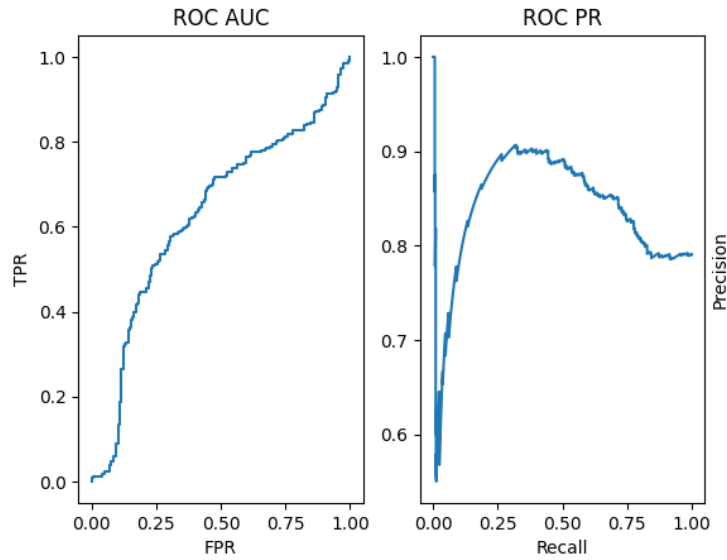


Figure 26: Multimodal sensor features with LOPO, binary classification: Gradient Boosting

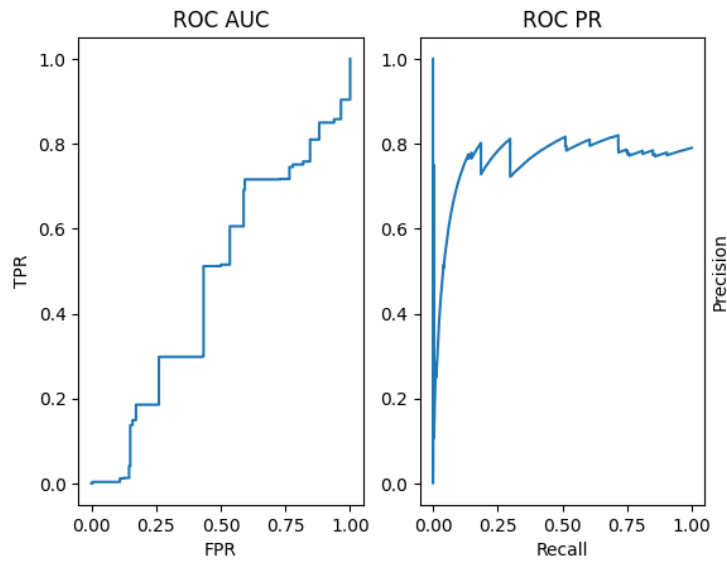


Figure 27: Multimodal sensor features with LOPO, binary classification: Catboost

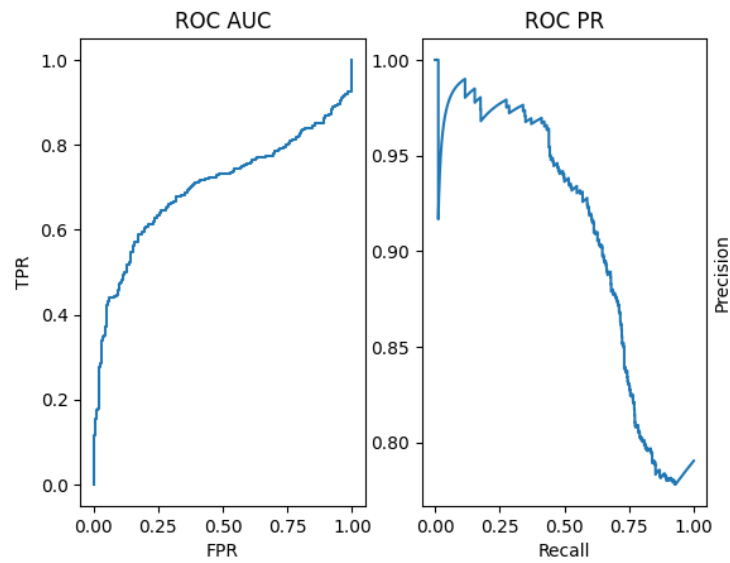


Figure 28: Multimodal sensor features with LOPO, binary classification: LightGBM

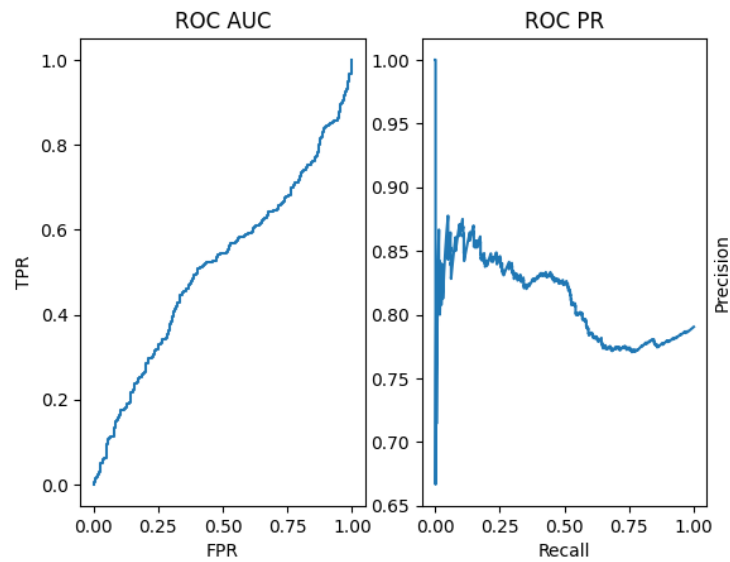


Figure 29: Multimodal sensor features with LOPO, binary classification: SVM

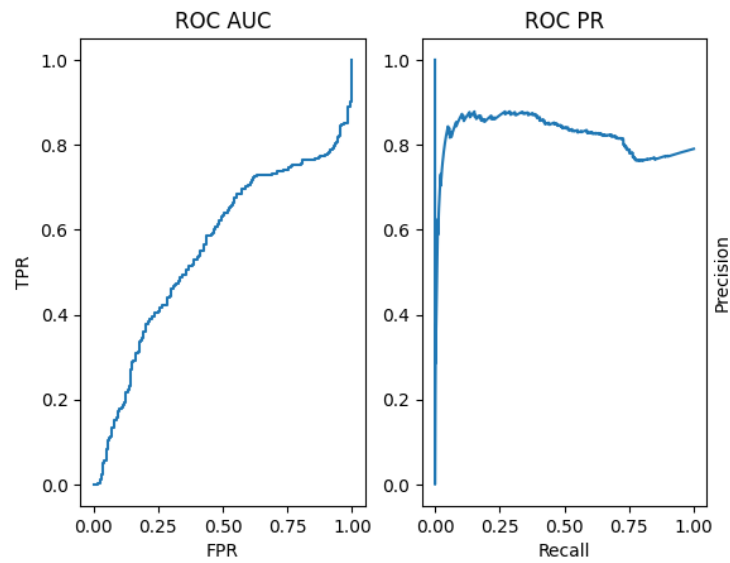


Figure 30: Multimodal sensor features with LOPO, binary classification: Random Forest

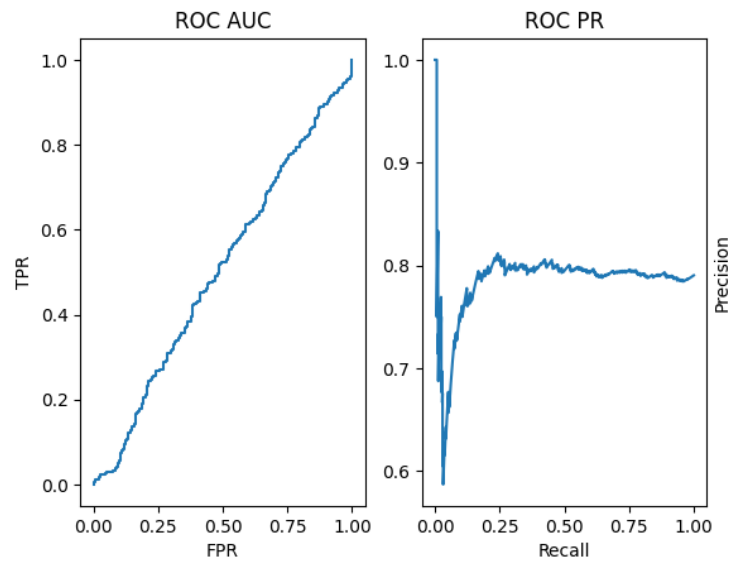


Figure 31: Multimodal sensor features with LOPO, binary classification: MLP

### E.3.2 Binary classification: K-folds

Figure 32, 33, 34, 35, 36, 37 shows the ROC AUC and ROC PR plots for multimodal sensor features binary classification models using Gradient Boosting, Catboost, LightGBM, SVM, Random Forest, and MLP respectively, with a K-folds split. These figures are plots from Table 12 in Section 4.3.

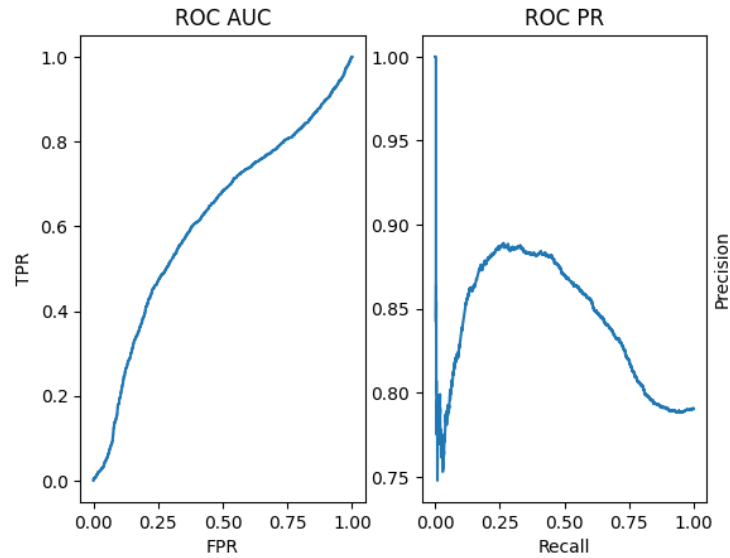


Figure 32: Multimodal sensor features with K-folds, binary classification: Gradient Boosting

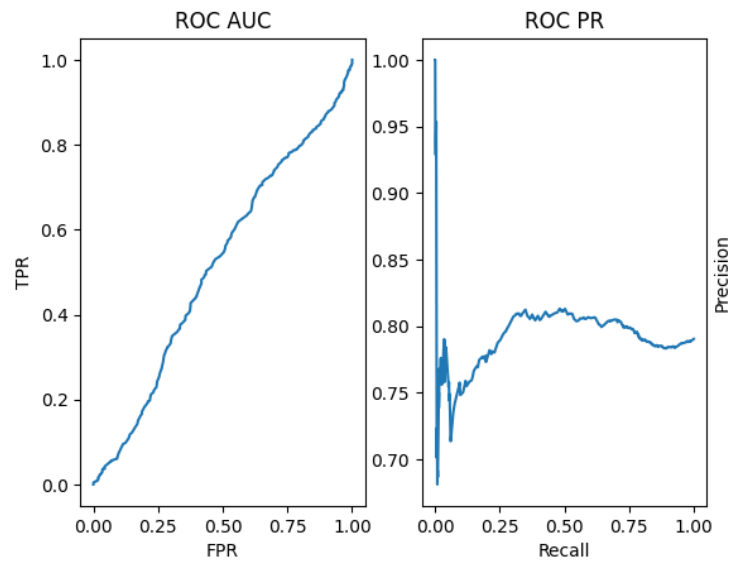


Figure 33: Multimodal sensor features with K-folds, binary classification: Catboost

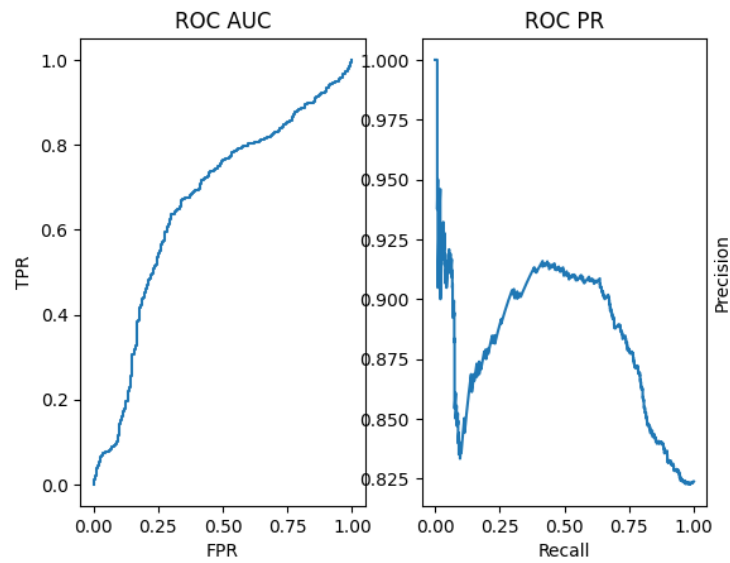


Figure 34: Multimodal sensor features with K-folds, binary classification: LightGBM

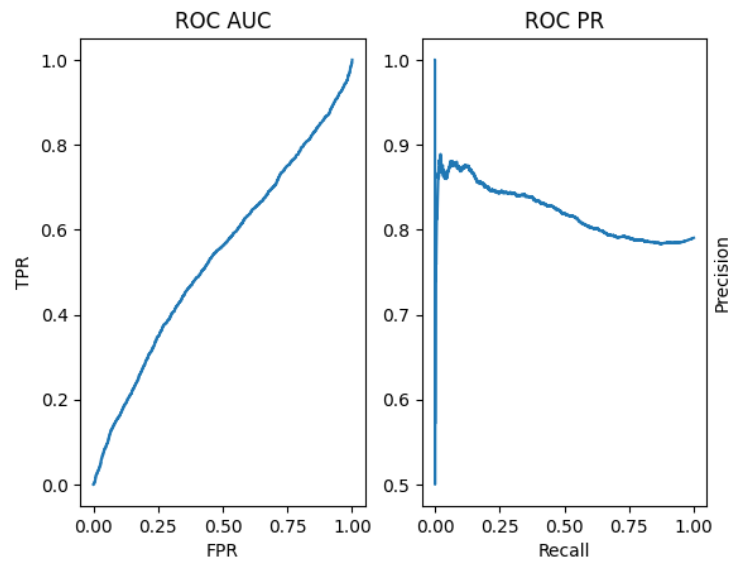


Figure 35: Multimodal sensor features with K-folds, binary classification: SVM



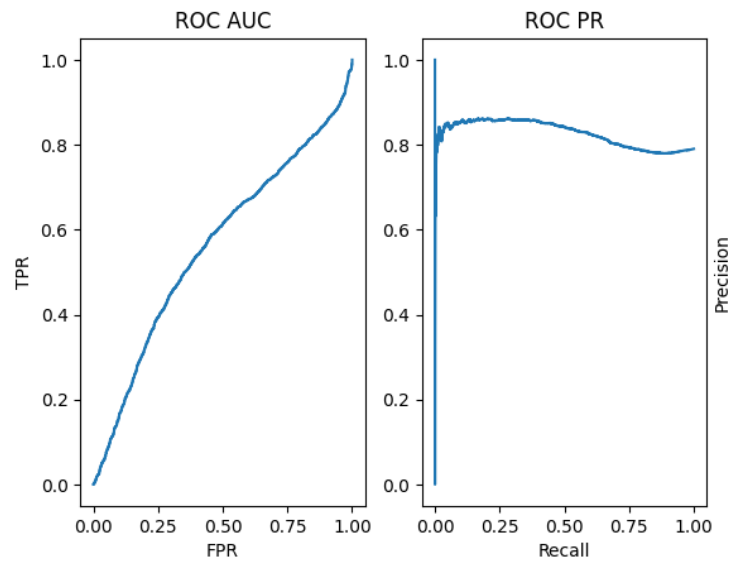


Figure 36: Multimodal sensor features with K-folds, binary classification: Random Forest

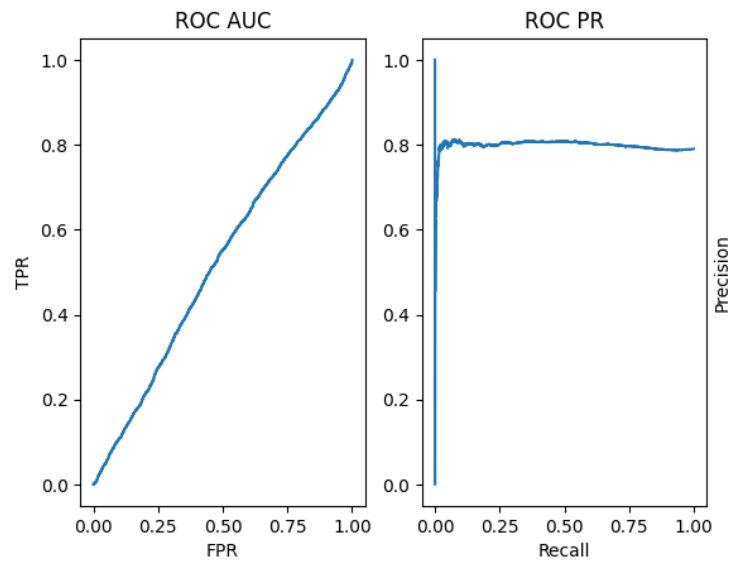


Figure 37: Multimodal sensor features with K-folds, binary classification: MLP

## E.4 Using Top-10 important features classification

### E.4.1 Binary classification: LOPO

Figure 38, 39, 40, 41, 42, 43 shows the ROC AUC and ROC PR plots for top 10 features binary classification models using Gradient Boosting, Catboost, LightGBM, SVM, Random Forest, and MLP respectively, with a LOPO split. These figures are plots from Table 13 in Section 4.4.

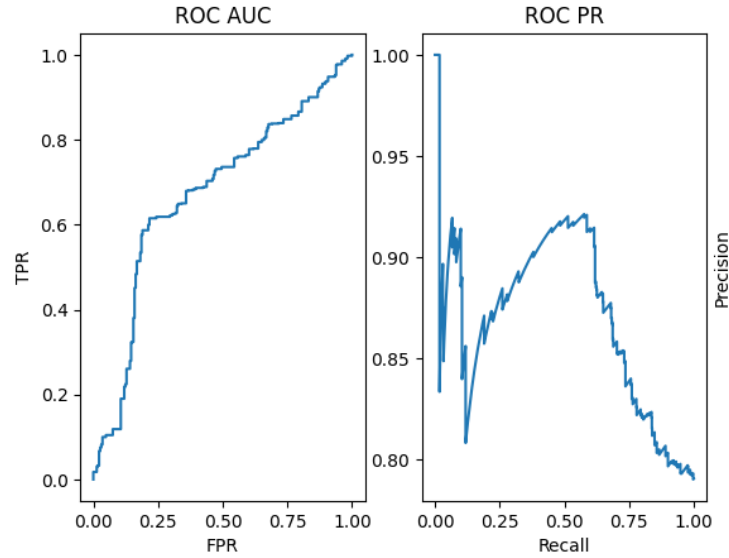


Figure 38: Top 10 features with LOPO, binary classification: Gradient Boosting

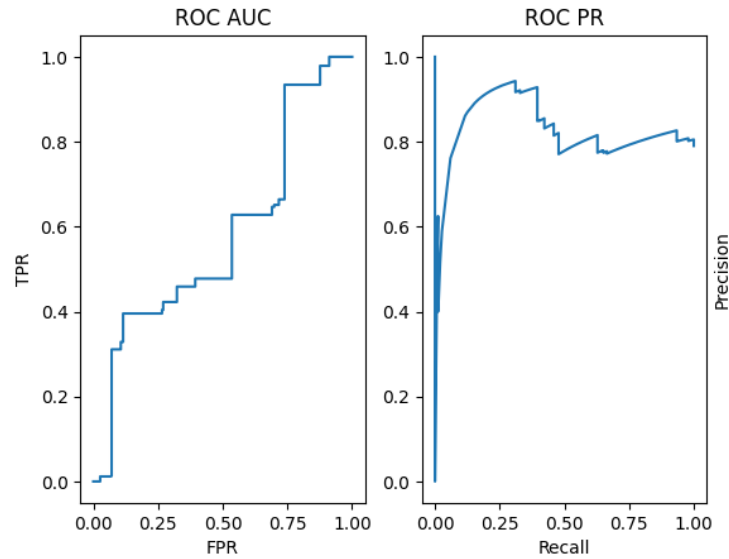


Figure 39: Top 10 features with LOPO, binary classification: Catboost

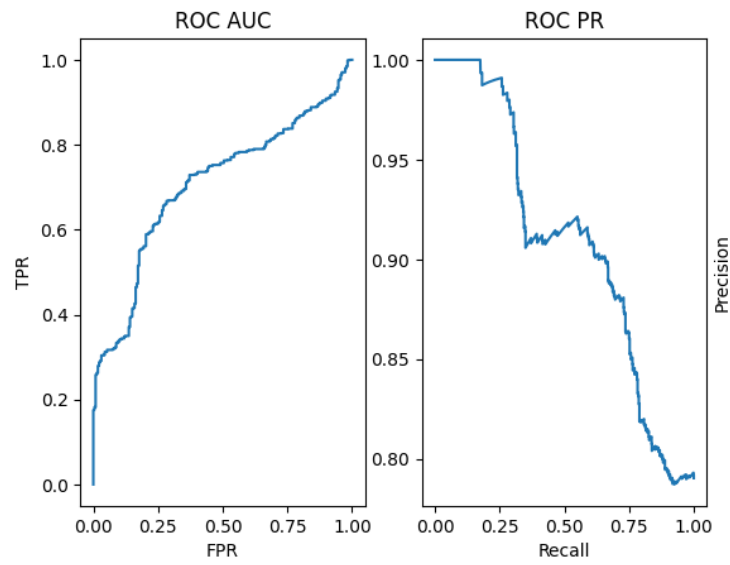


Figure 40: Top 10 features with LOPO, binary classification: LightGBM

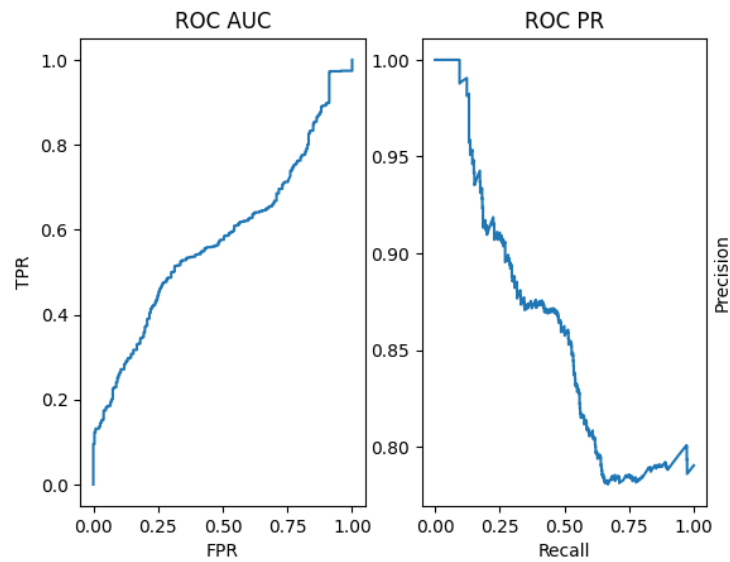


Figure 41: Top 10 features with LOPO, binary classification: SVM

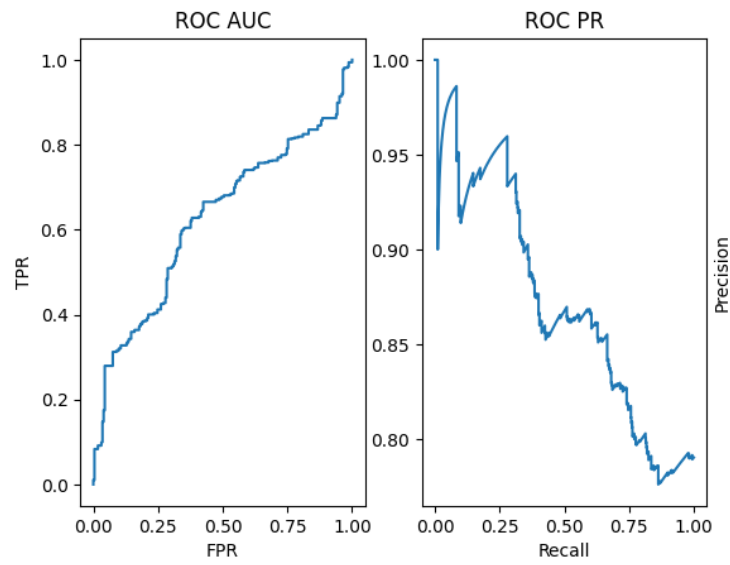


Figure 42: Top 10 features with LOPO, binary classification: Random Forest

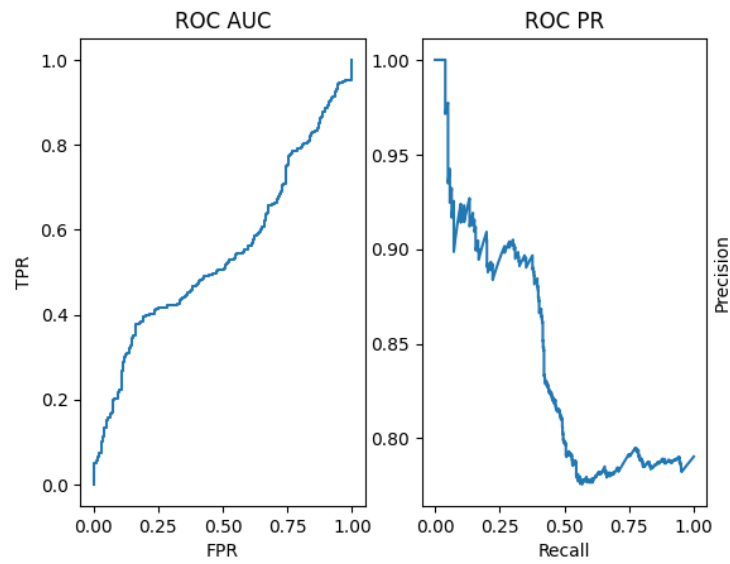


Figure 43: Top 10 features with LOPO, binary classification: MLP

### E.4.2 Binary classification: K-folds

Figure 44, 45, 46, 47, 48 shows the ROC AUC and ROC PR plots for top 10 features binary classification models using Gradient Boosting, Catboost, LightGBM, SVM, Random Forest, and MLP respectively, with a K-folds split. These figures are plots from Table 14 in Section 4.4.

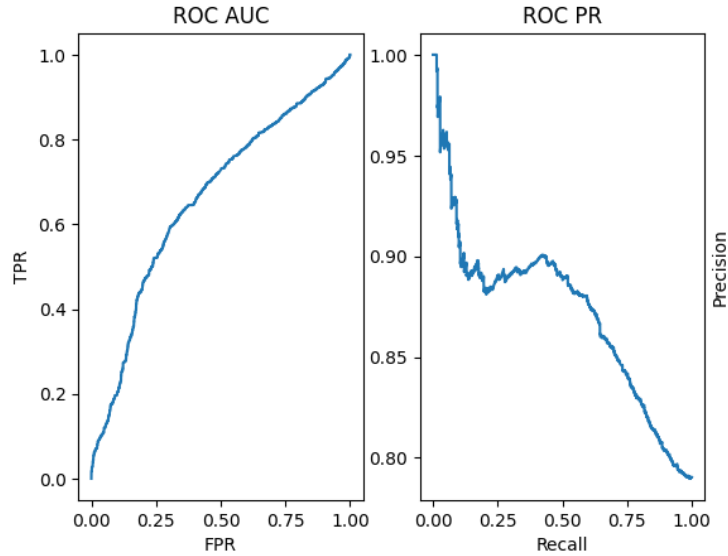


Figure 44: Top 10 features with K-folds, binary classification: Gradient Boosting

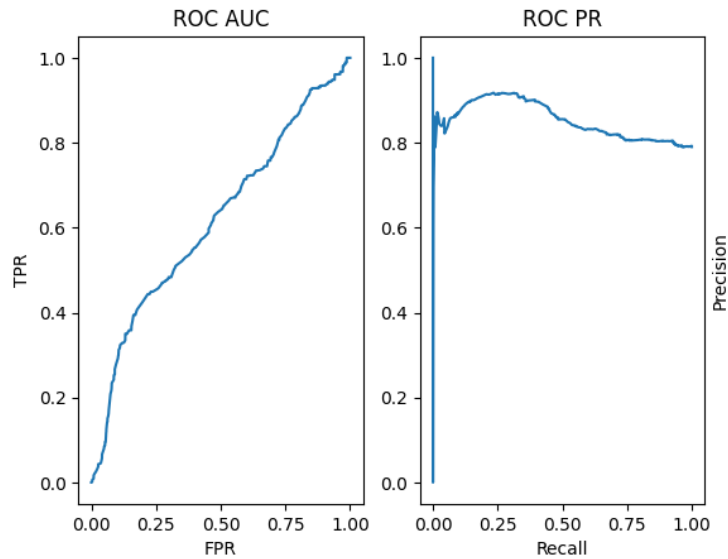


Figure 45: Top 10 features with K-folds, binary classification: Catboost

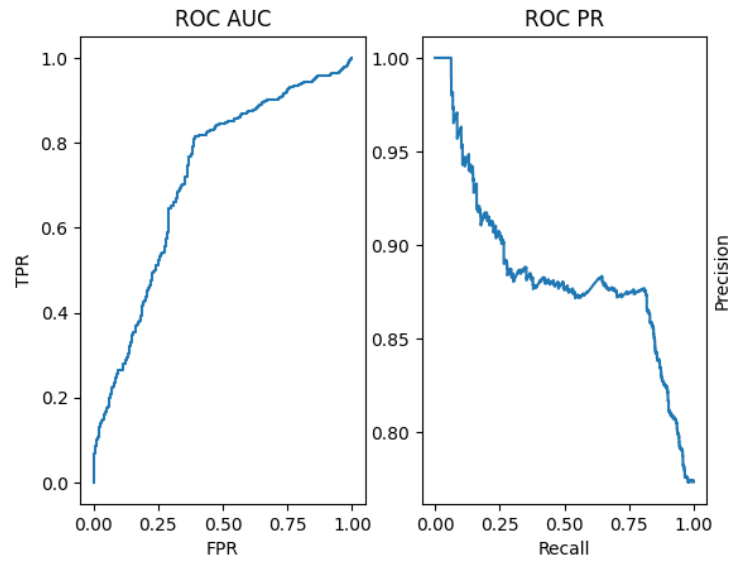


Figure 46: Top 10 features with K-folds, binary classification: LightGBM

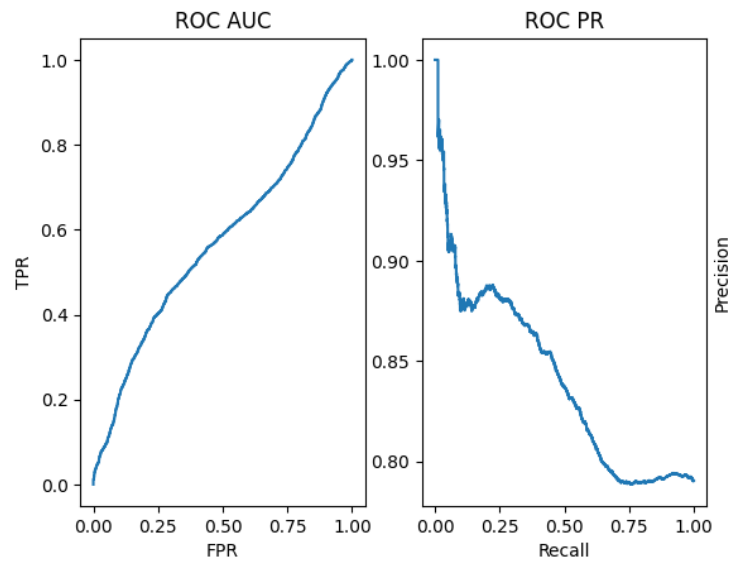


Figure 47: Top 10 features with K-folds, binary classification: SVM

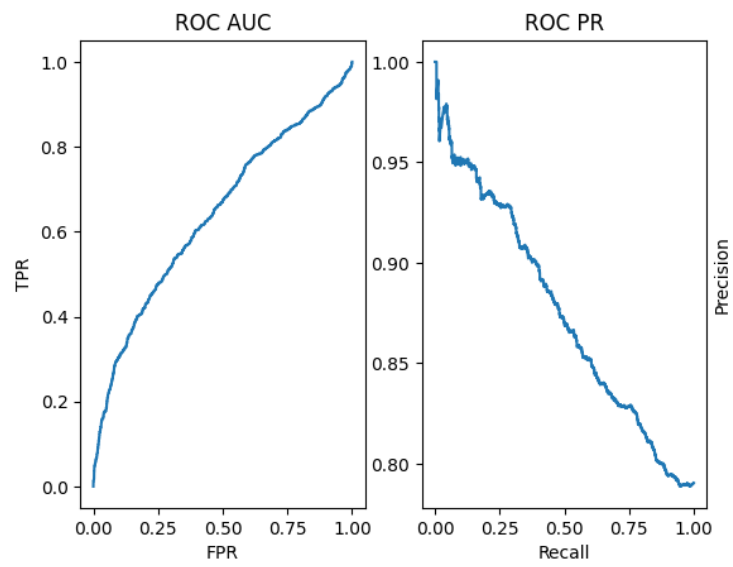


Figure 48: Top 10 features with K-folds, binary classification: Random Forest